Intraflagellar transport-A deficiency attenuates ADPKD in a renal tubular- and maturation-dependent manner

Wei Wang[1], Luciane M. Silva[1], Henry H. Wang[1], Matthew A. Kavanaugh[1], Tana S. Pottorf[1], Bailey A. Allard[1], Damon T. Jacobs[1], Rouchen Dong[1], Joseph T. Cornelius[1], Aakriti Chaturvedi[1], Michele T. Pritchard[2], Madhulika Sharma[3], Chad Slawson[4], Darren P. Wallace[3], James P. Calvet[4], Pamela V. Tran[1]

[1]Dept. of Anatomy and Cell Biology, The Jared Grantham Kidney Institute, University of Kansas Medical Center, Kansas City, KS

[2]Dept. of Pharmacology, Toxicology and Therapeutics, The Jared Grantham Kidney Institute, University of Kansas Medical Center, Kansas City, KS

[3]Dept. of Internal Medicine, The Jared Grantham Kidney Institute, University of Kansas Medical Center, Kansas City, KS

[4]Dept. of Biochemistry and Molecular Biology, The Jared Grantham Kidney Institute, University of Kansas Medical Center, Kansas City, KS

Running Title: IFT-A dysfunction in ADPKD

Correspondence should be addressed to:

Pamela V. Tran

Department of Anatomy and Cell Biology and

The Jared Grantham Kidney Institute

University of Kansas Medical Center

3901 Rainbow Blvd., MS #3038

Kansas City, KS 66160

Tel: 913-945-7325

Fax: 913-588-2710

E-mail: ptran@kumc.edu

Key Words: PKD, mouse models, primary cilia, renal cystic disease, tubule, O-GlcNAc

Abstract

Primary cilia are sensory organelles that are built and maintained by intraflagellar transport (IFT) multi-protein complexes. Deletion of certain ciliary genes in Autosomal Dominant Polycystic Kidney Disease (ADPKD) mouse models markedly attenuates PKD severity, indicating that a component of cilia dysfunction may have potential therapeutic value. To broaden the role of ciliary dysfunction, here we investigate the role of global deletion of *Ift-A* gene, *Thm1*, in juvenile and adult ADPKD mouse models. In cyst-lining cells of both juvenile and adult ADPKD models, cortical collecting duct cilia lengths and cytoplasmic and nuclear levels of the nutrient sensor, O-linked β-N-acetylglucosamine (O-GlcNAc) were increased. Relative to juvenile *Pkd2* conditional knock-out mice, deletion of *Thm1* together with *Pkd2* both increased and reduced cystogenesis in a tubule-specific manner without altering kidney function, inflammation, cilia lengths, and ERK, STAT3 and O-GlcNAc signaling. In contrast, *Thm1* deletion in adult ADPKD mouse models markedly attenuated almost all features of PKD, including renal cystogenesis, inflammation, cilia lengths, and ERK, STAT3 and O-GlcNAc signaling. These data suggest that differential factors in the microenvironments between renal tubules and between developing and mature kidneys influence cilia and ADPKD pathobiology. Further, since O-GlcNAcylation directly regulates ciliary homeostasis and the balance between glycolysis and oxidative phosphorylation, we propose that increased O-GlcNAcylation may promote certain key ADPKD pathological processes.

Introduction

Autosomal Dominant Polycystic Kidney Disease (ADPKD) is among the most common, fatal monogenetic diseases, affecting approximately 1:1000 individuals worldwide[1]. ADPKD is characterized by the growth of large fluid-filled renal cysts, which cause injury and fibrosis and can lead to end-stage renal disease by the 6th decade of life. Tolvaptan is the only FDA-approved therapy, but has variable effectiveness and aquaresis side effects[2, 3]. Thus, the need to discover additional underlying disease mechanisms and design new therapeutic strategies continues.

Primary cilia are small, antenna-like sensory organelles that play an important role in ADPKD pathobiology via mechanisms that remain unclear. ADPKD is caused by mutations in *PKD1* (≥80% of cases) or *PKD2* (≥10% of cases), which encode polycystin 1 (PC1) and polycystin 2 (PC2), respectively[4]. PC1 and PC2 form an ion-channel receptor complex that functions at the primary cilium. While PC1 and PC2 also localize to other subcellular compartments, analyses of human ADPKD primary renal epithelial cells, of mouse models harboring human ADPKD mutations, and of an ethylnitrosourea (ENU)-induced *Pkd2* mouse mutation that causes ciliary exclusion of PC2, indicate that deficiency of PC1 or PC2 from the cilium is sufficient to cause ADPKD[5-7].

Primary cilia are synthesized and maintained via intraflagellar transport (IFT), which is the bi-directional transport of protein cargo along a microtubular axoneme. Two multiprotein complexes mediate IFT. The IFT-B complex interacts with the kinesin motor and mediates anterograde IFT, while the IFT-A complex together with cytoplasmic dynein mediates retrograde IFT. IFT-A proteins are also required for ciliary import of membrane and signaling molecules[8-10]. In mice, deletion of *Ift-A* or *-B* genes either perinatally or in the embryonic kidney results in renal cystic disease[11-13]. However, these mutants differ from ADPKD models in manifesting generally smaller renal cysts and greater fibrosis relative to cyst size[14, 15]. Additionally, *Ift-A* and *–B* mutants differ in cilia phenotype - shortened and absent cilia, respectively - and can also show opposing signaling phenotypes, reflecting the differing

functions of IFT-A and -B[12, 16-18]. Intriguingly, deletion of *Ift-B* genes, *Kif3a, Ift20* and *Ift88*, and of an IFT-A adaptor gene, *Tulp3*, in *Pkd1* or *Pkd2* conditional knock-out (cko) mice reduces severity of the PKD phenotype[19-22], indicating that a component of cilia dysfunction has potential therapeutic value.

A commonly mutated *IFT* gene is *THM1* (TPR-containing Hedgehog modulator 1; also termed *TTTC21B*). Causative and modifying mutations in *THM1* have been identified in 5% of patients with ciliopathies, including nephronophthisis, Bardet Biedl syndrome, Meckel syndrome and Jeune syndrome[14]. *THM1* encodes an IFT-A component, and its deletion impairs retrograde IFT, causing accumulation of proteins in bulb-like distal tips of shortened primary cilia[16]. *Thm1* loss also impairs cilia entry of membrane-associated proteins, delays and reduces ciliogenesis, and promotes serum-induced cilia loss[23]. In mice, *Thm1* deletion recapitulates many of the clinical manifestations of ciliopathies[16, 24, 25]. Perinatal global deletion of *Thm1* results in renal cystic disease[24], while deletion of *Thm1* in adult mice does not result in a renal phenotype by 3 months of age, consistent with the developmental time-frame that determines whether loss of a cystogenic gene will cause rapid- or slow-progressing renal cystic disease[26]. To expand on the role of ciliary dysfunction in ADPKD, here we investigate the role of *Thm1*/ IFT-A deficiency in juvenile and adult ADPKD mouse models.

Methods

Generation of mice

Pkd1$^{flox/flox}$, *Pkd2*$^{flox/flox}$ and *ROSA26-Cre* mice were obtained from the Jackson Laboratories (Stock numbers 010671, 017292 and 004847, respectively). Generation of *Thm1* cko mice has been described previously[24]: *Thm1*$^{aln/+}$; *ROSA26Cre*$^{ERT+}$ male mice were mated to *Thm1*$^{flox/flox}$ females. *Pkd1* floxed alleles were introduced into the colony to generate *Thm1*$^{flox/flox}$;*Pkd1*$^{flox/flox}$ or *Thm1*$^{flox/flox}$;*Pkd1*$^{flox/+}$ females and *Pkd1*$^{flox/flox}$; *Thm1*$^{aln/+}$, *ROSA26-Cre*$^{ERT/+}$ males, which were mated. Similarly, *Pkd2* floxed alleles were introduced into the colony to generate *Thm1*$^{flox/flox}$;*Pkd2*$^{flox/flox}$ or *Thm1*$^{flox/flox}$;*Pkd2*$^{flox/+}$ females and *Pkd2*$^{flox/flox}$; *Thm1*$^{aln/+}$, *ROSA26-Cre*$^{ERT/+}$ males. To generate early-

onset *Pkd2* models, *Thm1*$^{flox/flox}$;*Pkd2*$^{flox/flox}$ or *Thm1*$^{flox/flox}$;*Pkd2*$^{flox/+}$ nursing mothers mated to *Pkd2*$^{flox/flox}$; *Thm1*$^{aln/+}$, *ROSA26-Cre*$^{ERT/+}$ males were injected intraperitoneally with tamoxifen (10mg/40g; Sigma) at postnatal day 0 (P0) to induce gene deletion. Offspring were analyzed at P21. To generate late-onset *Pkd1* models, offspring from matings between *Thm1*$^{flox/flox}$;*Pkd1*$^{flox/flox}$ or *Thm1*$^{flox/flox}$;*Pkd1*$^{flox/+}$ females and *Pkd2*$^{flox/flox}$; *Thm1*$^{aln/+}$, *ROSA26-Cre*$^{ERT/+}$ males were injected intraperitoneally with tamoxifen (10mg/40g) at P35. To generate late-onset *Pkd2* models, offspring from matings between *Thm1*$^{flox/flox}$;*Pkd2*$^{flox/flox}$ or *Thm1*$^{flox/flox}$;*Pkd2*$^{flox/+}$ females and *Pkd2*$^{flox/flox}$; *Thm1*$^{aln/+}$, *ROSA26-Cre*$^{ERT/+}$ males were injected intraperitoneally with tamoxifen (10mg/40g) at P28. Mice were analyzed at 6 months of age. All mouse lines were maintained on a pure C57BL6/J background (backcrossed 10 generations). All animal procedures were conducted in accordance with KUMC-IACUC and AAALAC rules and regulations.

Kidney and body weight measurements

Kidneys were dissected and weighed using a standard laboratory weighing scale. The kidney weight/body weight (KW/BW) ratio was calculated as the total kidney weights divided by body weight for each mouse.

Blood Urea Nitrogen Measurements

Mouse trunk blood was collected in Microvette CB 300 Blood Collection System tubes (Kent Scientific), and centrifuged at 1800g at room temperature for 10 minutes to collect serum. BUN was measured using the QuantiChrom Urea Assay Kit (BioAssay Systems) according to the manufacturer's protocol.

Histology

Kidneys were bisected transversely, fixed in 10% formalin for several days, then processed in a tissue processor and embedded in paraffin. Tissue sections (7μm) were obtained with a microtome. Sections were deparaffinized, rehydrated through a series of ethanol washes, stained with hematoxylin and eosin (H&E), rehydrated, then mounted using Permount (ThermoFisher). Images were taken with a Nikon 80i microscope equipped with a Nikon DS-Fi1 camera. Cystic areas of H&E-stained sections were quantified using ImageJ.

Immunofluorescence

Following deparaffinization and rehydration, tissue sections were subjected to an antigen retrieval protocol. Tissue sections were steamed for 15 minutes in Sodium Citrate Buffer (10 mM Sodium Citrate, 0.05% Tween 20, pH 6.0), returned to room temperature, rinsed 10 times in distilled water, washed 5 minutes in PBS, incubated for 5 minutes in 1% SDS in PBS based on a method by Brown et al., 1996[27], then washed 3 times in PBS. Sections were blocked with 1% BSA in PBS for 1 hour at room temperature, and then incubated with primary antibodies against acetylated-α tubulin (1:4000; Sigma, T7451), IFT81 (1:200; Proteintech, 11744-1-AP), αSMA (1:500; Abcam, ab5694), F4/80 (1: 400, Cell Signaling, 30325) and PCNA (1:300; Cell Signaling Technology, 13110), P-ERK (1:200; Cell Signaling, 4370); THP (1:100; Santa Cruz Biotechnology, sc-271022) overnight at 4°C in the presence or absence of lectins, DBA (1:100; Vector Laboratories, FL-1031) or LTL (1:300, Vector Laboratories, FL-1321). Sections were washed three times in PBS, and then incubated with secondary antibodies conjugated to Alexa Fluor 488 (1:500; Invitrogen, A-11001 (anti-mouse) or A-11034 (anti-rabbit)) or Alexa Fluor 594 (1:500; Invitrogen, A-11005 (anti-mouse) or A-11012 (anti-rabbit)) for 1 hour at room temperature. After three washes of PBS, sections were mounted with DAPI Fluoromount-G (Electron Microscopy Sciences). Staining was visualized and imaged using a Nikon 80i microscope with a photometrics camera or a Nikon Eclipse TiE attached to an A1R-SHR confocal, with an A1-DU4 detector, and LU4 laser launch.

Immunohistochemistry

Tissue sections were deparaffinized, rehydrated, and subjected to antigen retrieval, which consisted of steaming sections for 25 minutes in Sodium Citrate Buffer (10 mM Sodium Citrate, 0.05% Tween 20, pH 6.0). Sections were treated with 3% hydrogen peroxide for 30 min to minimize background staining, washed in PBS, then blocked with 1% BSA for 1 hour. Tissue sections were incubated with primary antibodies against P-STAT3 (1:50; GeneTex, GTX118000), O-GlcNAc (1:200; ThermoFisher, RL2, MA1-072), OGT (1:200; a kind gift from Jerry Hart, UGA) and OGA (1:2000; a kind gift from Jerry Hart, UGA) overnight at 4^0C. Sections were washed three times in PBS, then incubated with HRP-conjugated rabbit secondary antibody (Cell Signaling) for 30 minutes. Sections were washed three times in PBS, incubated with ABC reagent (Vector Laboratories), rinsed in PBS, then incubated with SigmaFAST DAB metal enhancer (Sigma) until desired signal/color was obtained. Sections were counterstained with haemotoxylin, dehydrated through an ethanol series, and mounted with Permount (ThermoFisher). Staining was visualized and imaged using a Zeiss A1 microscope with a Axiocam 105 color camera.

Scanning electron microscopy

Small pieces of kidney cortices were fixed in 4% paraformaldehyde/2% glutaraldehyde, then washed three times in 0.1 M Na-cacodylate, pH 7.4. Samples were post-fixed for 30 minutes with 1% OsO4 in 0.1 M Na-cacodylate buffer, then dehydrated using an ethanol series, followed by hexamethyldisilazane (HMDS; Electron Microscopy Sciences). Samples were mounted onto metal stubs and sputter coated with gold. Samples were viewed and imaged using a Hitachi S-2700 Scanning Electron Microscope equipped with a Quartz PCI digital capture.

qPCR

RNA was extracted using Trizol (Life Technologies), then reverse transcribed into cDNA using Quanta Biosciences qScript cDNA mix (VWR International). qPCR for *Ccl2* and *Oaz1*, a housekeeping gene, was performed using Quanta Biosciences Perfecta qPCR Supermix (VWR International) in a BioRad CFX Connect Real-Time PCR Detection System. Primers used were *mCcl2* (Forward: 5'-AAGCTCAACCCTGACTTCTTAC-3'; Reverse: 5'-CAACGTCTGAGAACTGGAGAAA-3') and *mOaz1* (Forward: 5'-GCCTGAGGGCAGTAAGGAC-3'; Reverse: 5'-GGAGTAGGGCGGCTCTGT-3'). qPCR was performed in duplicate using RNA lysates from five samples per genotype.

ADPKD and normal human kidney sections

Normal human kidneys (NHK) and ADPKD kidneys were obtained from the PKD Biomarkers, Biomaterials, and Cellular Models Core in the Kansas PKD Center. The protocol for the use of discarded human tissues complied with federal regulations and was approved by the Institutional Review Board at KUMC. Paraffin-embedded de-identified NHK, n=3 (K357, K402, K419), and ADPKD, n=3 (K386, K408, K423) tissues were sectioned. Sections were deparaffinized and rehydrated, steamed in Sodium Citrate Buffer (10 mM Sodium Citrate, 0.05% Tween 20, pH 6.0) for antigen retrieval, and immunostained for ARL13B (1:300; Proteintech, 17711-1-AP).

Statistics

GraphPad Prism 8 software was used to perform statistical analyses. Statistical significance was determined as $p<0.05$. For analysis of more than two groups, one-way ANOVA followed by Tukey's test or a Kriskall-Wallis test were used to analyze data with or without normal distribution, respectively. For analysis of two groups, an unpaired t-test was used.

Results

Perinatal deletion of *Thm1* in *Pkd2* conditional knock-out mice reduces cortical cystogenesis, but does not improve kidney function

To examine the effect of IFT-A deficiency in an early-onset, rapidly progressing ADPKD mouse model, we deleted *Thm1* together with *Pkd2* at postnatal day (P) 0, and examined the renal phenotypes of control, *Thm1* conditional knock-out (cko), *Pkd2* cko and *Pkd2;Thm1* double knock-out (dko) mice at P21. At this early stage, *Thm1* cko kidneys on a pure C57BL6/J background appeared mostly intact morphologically, with some tubular dilations observed in the cortex and with kidney weight/body weight (KW/BW) ratios similar to control (Figures 1A and 1B). Yet BUN levels were elevated about 2-fold (Figure 1C). In *Pkd2* cko mice, renal cysts are present in both cortex and medulla, and KW/BW ratios and BUN levels are increased 5- and 3-fold, respectively. In *Pkd2;Thm1* dko mice, renal cysts are also present in the cortex and medulla, and KW/BW ratios and BUN levels are increased 4- and 3-fold, respectively. Thus relative to *Pkd2* cko mice, *Pkd2;Thm1* dko mice have reduced KW/BW ratios, but similar kidney dysfunction. Also relative to *Pkd2* cko mice, *Pkd2;Thm1* dko kidneys show decreased percent cystic index (Figure 1D), due to reduced cystogenesis in the cortex (Figure 1E), while cystogenesis in the medulla was similar (Figure 1F).

Perinatal deletion of *Thm1* in *Pkd2* conditional knock-out mice reduces cortical collecting duct cystogenesis, but increases proximal tubular and glomerular dilations

Since cortical cystogenesis was reduced in *Pkd2;Thm1* dko kidneys relative to *Pkd2* cko kidneys, we further analyzed the cortical cysts. At P21 in the *Thm1* cko renal cortex, we observed some dilations, most of which were LTL+, marking proximal tubules, and fewer that were THP+ or DBA+, marking loop of Henle and collecting duct, respectively (Figure 1G). In *Pkd2* cko renal cortex, LTL+ dilations, THP+ cysts, and multiple, large DBA+ cysts were observed. In *Pkd2; Thm1* dko cortex, LTL+ dilations were increased relative to those of *Pkd2* cko and *Thm1* cko kidneys (Figures 1G

and 1H); THP+ cysts were similar in size to those of *Pkd2* cko kidneys (Figure 1G; relative percent THP+ cystic index of *Pkd2* cko vs. dko mean ± sd is 1.0 ± 0.4 vs. 0.9 ± 0.1; *Pkd2* cko mean value set at 1.0; n=4; not significant); and DBA+ cysts were decreased in size relative to those of *Pkd2* cko kidneys (Figures 1G and 1I). We also observed glomerular dilations in the mutant kidneys (Figure 1J). To quantify glomerular dilations, percentage of area of Bowman's space over the area of glomerular tuft was calculated. In *Pkd2* cko kidneys, this percentage was increased, and in *Pkd2;Thm1* dko kidneys, this percentage was further increased relative to *Pkd2* cko kidneys, indicating that additional loss of *Thm1* exacerbates *Pkd2* cko glomerular dilations (Figure 1K). These differences reveal that the role of *Thm1* deletion on a *Pkd2* cko background is specific to the nephron segment.

Deletion of *Thm1* alone increases inflammation

Proliferation is a cellular hallmark of ADPKD renal cystogenesis. We therefore immunostained for Proliferating cell nuclear antigen (PCNA) together with proximal tubule and collecting duct markers, LTL and DBA, respectively. In LTL+ tubules, PCNA levels were similar across control, *Thm1* cko and *Pkd2* cko kidneys, and slightly elevated in *Pkd2;Thm1* dko kidneys (Figures 2A-2B). However, PCNA+ cells were increased in *Pkd2* cko and *Pkd2;Thm1* dko DBA+ tubules, and further increased in *Pkd2* cko and *Pkd2;Thm1* dko DBA+ cysts (Figure 2C). These data support that increased proliferation is an early driver of ADPKD renal cystogenesis.

Cyst growth compresses surrounding parenchyma, leading to injury, inflammation, and fibrosis. We immunostained kidney sections for alpha smooth muscle actin (αSMA) and F4/80 to examine the presence of myofibroblasts and macrophages, respectively, which contribute to pro-inflammatory and pro-fibrotic processes. In control kidneys, αSMA was present around blood vessels and few F4/80+ cells were present (Figure 2D). In *Thm1* cko kidneys, αSMA localized around blood vessels, in addition to around glomeruli and tubular dilations, and number of F4/80+ cells was

increased. In *Pkd2* cko and *Pkd2;Thm1* dko kidneys, even more αSMA+ and F4/80+ labelling was observed surrounding glomeruli, tubular dilations and cysts. Thus, deletion of *Thm1* alone increases inflammatory processes, but its deletion on a *Pkd2* cko background does not exacerbate ADPKD inflammation at P21.

Deletion of *Pkd2* increases cilia length on renal epithelia

We next examined primary cilia on renal tubular epithelia by co-immunostaining for acetylated, α-tubulin together with LTL or DBA. In control kidneys, average cilia lengths were 3.0μm and 2.1μm for LTL+ and DBA+ cells, respectively (Figures 2E-2H). We also noted qualitative differences between LTL+ and DBA+ primary cilia, with the former cilia being thinner and longer, and the latter being thicker and more rod-like. Cilia lengths were increased in both *Pkd2* cko LTL+ and DBA+ tubules. However, relative to *Pkd2* cko tubules, cilia lengths were further increased in *Pkd2;Thm1* dko LTL+ tubules, but similar in *Pkd2;Thm1* dko DBA+ tubules. These differences reveal tubular-specific effects on cilia length.

Perinatal deletion of *Thm1* increases ERK and STAT3 signaling

Primary cilia mediate signaling pathways. Thus, we next examined signaling pathways, ERK and STAT3, which promote disease progression in ADPKD[28-31] and which we have observed can be regulated by *Thm1 in vitro* (data now shown). Low intracellular Ca^{2+} and high cAMP activates ERK signaling, which promotes cell proliferation[30, 32] and also acts upstream of mTOR and AMPK pathways regulating cellular metabolism[33]. Full-length and cleaved PC1 can directly activate STAT3, which can have proliferative and inflammatory roles[31, 34, 35]. We immunostained for P-ERK together with either LTL or DBA. At P21, P-ERK did not localize with LTL, but localized with DBA (Figure 3A). While a similar number of P-ERK+ tubules was observed across control and the various mutant

genotypes (Figure 3B), P-ERK intensity was increased in dilated tubules of *Thm1* cko mice, and further increased in cyst-lining cells of *Pkd2* cko and *Pkd2;Thm1* dko mice (Figure 3C). These data support that ERK activation is a driver of renal cyst growth. Using immunohistochemistry, P-STAT3 was revealed to be increased in epithelial cells lining cortical dilations in *Thm1* cko kidneys and to be further increased in cyst-lining cells of *Pkd2* cko and *Pkd2;Thm1* dko kidneys, both in the cortex and medulla (Figure 3E). Thus, dilations caused by *Thm1* loss as well as *Pkd2* cystic disease cause increased ERK and STAT3 signaling.

O-GlcNAcylation is increased in dilated tubules and cysts

Altered cellular metabolism has emerged as an important component of ADPKD pathobiology[33, 36-38]. One of these alterations includes the Warburg effect[33], whereby cells preferentially convert the product of glycolysis, pyruvate, into lactate, even in the presence of oxygen. This pathway yields much less ATP than the entry of pyruvate in mitochondria, generating ATP via oxidative phosphorylation. The nutrient sensor, O-linked β-N-acetylglucosamine (GlcNAc) regulates the balance between glycolysis and oxidative phosphorylation[39], as well as ciliary homeostasis[40, 41], both of which are altered in ADPKD[33, 42]. We therefore examined O-GlcNAc signaling. In control kidneys, immunohistochemistry for O-GlcNAc revealed mostly nuclear staining in tubules of the cortex, and lesser staining in tubules of the medulla (Figure 4A). In *Thm1* cko kidneys, O-GlcNAc expression was increased in nuclei of cells lining dilations in the cortex, but similar to control in the medulla. In *Pkd2* cko kidneys, OGlcNAc staining was intense in cyst-lining cells in both the cortex and medulla. Relative to *Pkd2* cko kidneys, *Pkd2;Thm1* kidneys showed slightly reduced O-GlcNAc staining in cyst-lining cells of the cortex, but similar staining in the medulla. O-GlcNAC is regulated by two enzymes, O-GlcNAc transferase (OGT) and O-GlcNAcase (OGA), which respectively transfers and removes the O-GlcNAc moiety on protein substrates. In control kidneys, low expression of OGT

was present in the cytoplasm of tubular epithelia in the cortex and medulla (Figure 4B). In *Thm1* cko kidneys, OGT was increased in the cytoplasm and nuclei of cells lining dilations in the cortex, while OGT levels were similar to control in the medulla. In *Pkd2* cko and in *Pkd2;Thm1* dko mice, intense OGT staining was present in cyst-lining cells in the cortex and medulla. In control kidneys, OGA staining was present in the cytoplasm of proximal tubule cells and even lighter cytoplasmic stain was present in the medullary tubules (Figure 4C). In *Thm1* cko kidneys, OGA staining was similar to control. In *Pkd2* cko and in *Pkd2;Thm1* dko mice, OGA was increased in the nuclei and cytoplasm of cyst-lining cells in both the cortex and medulla. Together, these data suggest that misregulation of O-GlcNAc signaling may contribute to renal cystogenesis.

Deletion of *Thm1* in adult *Pkd2* or *Pkd1* conditional knock-out mice markedly attenuates ADPKD renal cystogenesis

We next examined the role of IFT-A deficiency in late-onset, slowly progressive adult ADPKD mouse models. We deleted *Thm1* together with *Pkd1* at P35 and examined the renal phenotypes at 6 months of age. Late-onset *Thm1* cko kidneys have morphology and BUN levels similar to control kidneys (Figure S1A). In *Pkd1* cko mice, renal cysts were mostly in the cortex, with the largest and most abundant cysts being DBA+ (Figure 5A). Fewer cysts were THP+, and only dilations, not cysts, were observed that were LTL+. Notably, all these features were reduced in *Pkd1; Thm1* dko kidneys. KW/BW ratios were elevated in *Pkd1* cko mice, and corrected in *Pkd1;Thm1* dko mice (Figure 5B). Additionally, BUN levels were slightly elevated in *Pkd1* cko mice, while BUN levels in *Pkd1;Thm1* dko mice were similar to control (Figure 5C).

Since *PKD2* mutations result in less severe ADPKD, we deleted *Thm1* together with *Pkd2* at P28 and examined renal phenotypes at 6 months of age. *Thm1* cko kidneys have morphology and BUN levels resembling those of control mice (Figure S1B). *Pkd2* cko mice show renal cysts mostly in the cortex, with the largest cysts being DBA+, and smaller cysts being LTL+ or THP+ (Figure 5D). In

contrast, in *Pkd2;Thm1* dko mice, the *Pkd2* cko cystic phenotype is largely corrected morphologically. In *Pkd2* cko mice, KW/BW ratios were similar to control and BUN levels showed a trend toward a slight elevation, reflecting the mild disease induced in adulthood. In *Pkd2;Thm1* dko mice, KW/BW ratios were slightly reduced relative to control and *Pkd2* cko mice, due to increased body weight caused by global deletion of *Thm1*[25]. In *Pkd2;Thm1* dko mice, BUN levels showed a slight decreasing pattern relative to *Pkd2* cko mice.

Deletion of *Thm1* in adult ADPKD mouse models results in reduced cilia length of cortical collecting duct renal epithelia

Similar to juvenile ADPKD models, cilia lengths measured by immunostaining for acetylated α-tubulin, were increased in *Pkd1* cko and *Pkd2* cko DBA+ adult tubules (Figures 5G, 5H, 5J, and 5K). However, in contrast to juvenile models, cilia lengths of *Pkd1;Thm1* and *Pkd2;Thm1* dko DBA+ tubular epithelia were reduced relative to those of *Pkd1* cko and *Pkd2* cko epithelia and similar to control. Additionally, human ADPKD sections had longer epithelial cilia than NHK sections (Figures 5I and 5L), supporting that increased cilia length is also a feature of the human disease.

Deletion of *Thm1* in adult *Pkd1* conditional knock-out mice reduces proliferation, inflammation, P-ERK, P-STAT3, and O-GlcNAc

To further assess the extent of ADPKD attenuation by *Thm1* deletion, we examined proliferation and inflammation in late-onset *Pkd1* cko and *Pkd1;Thm1* dko mice. In *Pkd1* cko kidneys, PCNA was expressed in cyst-lining cells (Figure 6A), αSMA was expressed around blood vessels, cysts as well as glomeruli (Figure 6B), while F4/80 was expressed surrounding cysts and glomeruli. Notably, in *Pkd1;Thm1* dko kidneys, PCNA was not expressed, αSMA was expressed around blood vessels, and F4/80+ cells were reduced and randomly dispersed throughout the kidney, resembling

control. Similar to in juvenile mice, P-ERK was not expressed in LTL+ cells, but was expressed in DBA+ tubular and cyst-lining epithelia (Figure 6C). P-ERK staining was more intense in *Pkd1* cko kidneys and reduced in *Pkd1;Thm1* dko kidneys. P-STAT3 was also increased in cyst-lining cells of *Pkd1* cko kidneys, and reduced in *Pkd1;Thm1* dko kidneys (Figure 6D). Additionally, pro-inflammatory cytokine, *Ccl2*[43], was elevated in *Pkd1* cko kidneys, but reduced in *Pkd1;Thm1* dko kidneys (Figure 6E). Thus, proliferative and pro-inflammatory pathways are attenuated in late-onset ADPKD by deletion of *Thm1*.

Using immunohistochemistry, we examined O-GlcNAcylation. In control kidneys, light cytoplasmic staining of O-GlcNAc was present in tubules of both the cortex and medulla. In *Pkd1* cko kidneys, increased O-GlcNAc occurred in cyst-lining epithelia of the cortex, in proteinaceous substances present in some of the cysts, and in tubules of the medulla (Figure 7A). In *Pkd1;Thm1* dko kidneys, O-GlcNAc staining was reduced, with light cytoplasmic expression in cortical tubules, similar to control, and with increased expression still present in some medullary tubules. In control kidneys, OGT and OGA were lightly expressed in the cytoplasm of tubular epithelia of both cortex and medulla (Figures 7B and 7C). In *Pkd1* cko kidneys, OGT and OGA were increased in the cytoplasm and nuclei of cyst-lining cells of the cortex and in some tubules of the medulla. In *Pkd1;Thm1* dko kidneys, OGT and OGA expression were similar to control. These data suggest that increased O-GlcNAcylation is a feature of late-onset ADPKD, similar to early-onset disease. Further, deletion of *Thm1* in late-onset ADPKD attenuates perturbation of this metabolic regulator.

Discussion

Primary cilia are key organelles in ADPKD pathobiology, through mechanisms that are poorly understood. Deleting IFT-B genes attenuates PKD severity in both juvenile and adult ADPKD models[19]. In contrast, deleting *Tulp3*, an IFT-A adaptor, attenuated renal cystic disease in an adult

ADPKD model only[21,44]. Since the attenuation of ADPKD with deletion of these ciliary genes is so striking, identifying the underlying mechanism could lead to a very effective therapeutic target.

Expanding the role of cilia dysfunction in ADPKD, we show that similar to *Tulp3*, deletion of IFT-A gene, *Thm1*, does not attenuate renal function in an early-onset ADPKD model, but markedly attenuates almost all aspects of ADPKD in a late-onset model (Figure 8). Yet distinct from *Tulp3*[44], global deletion of *Thm1* in an early-onset model reduces KW/BW ratios and cortical collecting duct cystogenesis. Our data further reveal that the effects of *Thm1* deletion on an early-onset ADPKD background are nephron-specific, with no effect on loop of Henle-derived cysts, and exacerbation of proximal tubular and glomerular dilations. This is the first demonstration that cilia dysfunction has differential effects on ADPKD tubules and may reflect varying microenvironments between nephron segments. The differential effects of *Tulp3* or *Thm1* deletion in early- versus late-onset ADPKD mouse models further suggest differences in developing versus mature renal microenvironments. Collectively, these data highlight the importance of renal context and examining molecules and pathways by cell type or at the single cell level in the kidney.

Embryonic mutation or perinatal loss of either *Kif3a*, *Ift88*, *Tulp3* or *Thm1* causes renal cystic disease[24, 21, 45, 46], suggesting that each of these genes is required for kidney development. Thus, their requirement for kidney development does not explain the differential effects in early-onset ADPKD. Instead, the differential effects may be due to differences in their specific cellular function, such as cilia length regulation, ciliary entry or transport of protein cargo, or regulation of signaling pathways. IFT-B and -A complexes regulate cilia length through different mechanisms. IFT-B genes mediate anterograde IFT, while IFT-A genes and *Thm1* mediate retrograde IFT as well as ciliary entry of membrane and signaling proteins. In contrast, *Tulp3* does not regulate cilia length, but is required for ciliary entry of membrane-associated and signaling molecules[44]. Additionally, IFT-B and -A mutants have shown opposing signaling phenotypes. Any of these functions can be explored to account for the differing early-onset dko phenotypes.

Increased cilia lengths on renal epithelia of several ADPKD mouse models, *PKD1*$^{RC/RC}$, *Pkd1* and *Pkd2* cko mice[47, 48], and recently, on human ADPKD tissue[22], have been reported. Our data substantiate that loss of polycystin function causes increased cilia length in mouse models as well as in human ADPKD, suggesting that ciliary mechanisms in the disease are likely conserved between mouse and human. Further, our data show that in addition to genotype, cilia structure varies by renal tubule segment and maturation, suggesting that factors within a tubule's microenvironment affect cilia length. Indeed, multiple factors including intracellular Ca^{2+} and cAMP, oxidative stress, cytokines, and fluid flow, affect cilia length of renal epithelial cells[49-51], indicating that cilia length may be finely regulated in order to maintain renal tubular structure and function. In support of an ameliorative effect of reduced cilia length in ADPKD, inhibition of cilia disassembly in *Pkd1* cko mice increased renal cilia length and exacerbated ADPKD[52], while in the *jck* non-orthologous PKD mouse model, which also has increased renal cilia lengths, pharmacological shortening of primary cilia was associated with attenuated PKD[53].

Reduced *Ccl2* and Wnt signaling in *Pkd; Ift-B* dko mice[20, 22], and reduced P53 enhancing cilia disassembly in *Pkd; Ift-B* dko cells[42] are potential mechanisms by which ablation or shortening of primary cilia attenuate ADPKD. In addition to detecting ligands, primary cilia also detect mechanical cues. Although mechanosensing by primary cilia and the polycystins has been controversial, recent studies have renewed interest in a potential mechanosensory role for the polycystins, particularly regarding tissue microenvironment stiffness[54, 55]. If sensing of physical forces in the tissue microenvironment is essential to maintaining renal tubular function, then other mechanical cues that would change with cyst growth include shear stress and intraluminal pressure. Cilia length itself could then also be a possible contributing factor in PKD severity. Supporting a role for cilia length, a recent study has shown that primary cilia of proximal tubule epithelial cells transduce shear stress into metabolic pathways that culminate in oxidative phosphorylation[56]. Finally, by extrapolating findings of

cilia studies from the cancer field[57], cilia of not only renal tubular epithelial cells, but of interstitial cells might also affect signaling and disease severity.

Our data are the first to reveal increased O-GlcNAcylation in cyst-lining renal epithelial cells of both early- and late-onset ADPKD mouse models, suggesting increased O-GlcNAcylation may be a feature of ADPKD. Increased O-GlcNAcylation is a pathologic feature of diabetic nephropathy[58, 59], and in rodent models, has shown to promote various aspects of chronic kidney disease[60, 61] and also renal fibrosis[62]. In contrast, in a mouse model of contrast-induced acute kidney disease, an acute increase in O-GlcNAcylation was protective[63], emphasizing important differences between chronic and acute increases in O-GlcNAcylation. While acute changes are adaptive and necessary to maintain cellular health and metabolism, chronic changes are likely to contribute to pathology[64]. Chronic elevation of O-GlcNAcylation in cancer cells promotes tumor growth, and cancer cells show the Warburg effect, suggesting similar cellular metabolic alterations between ADPKD and cancer. A recent study has demonstrated that O-GlcNAcylation of Phosphoglycerate kinase 1 (PGK1), which catalyzes the first ATP molecule in glycolysis, activates PGK1 to enhance lactate production and reduce mitochondrial oxidative phosphorylation, promoting the Warburg effect[39]. Perhaps a similar mechanism may occur in ADPKD cells.

OGT localizes to the pericentriolar region during the early phases of ciliogenesis[56], and perturbation of O-GlcNAcylation affects cilia length[40, 41]. Further, the ciliary structural defects caused by OGT inhibition suggest impaired centriole formation and IFT[56]. However, studies have shown opposing effects of OGT deficiency or inhibition on cilia length[40, 41], indicating further studies are required. Possible causes may include differences in cell type, degree of OGT deficiency, or feedback regulation between OGT and OGA[64]. Chronic hyper-O-GlcNAcylation in diabetic tissues results in ciliary defects[65], demonstrating a causative link between misregulation of O-GlcNAcylation and defective ciliary homeostasis in a disease context. Since increased renal cilia lengths are associated with ADPKD renal cystogenesis[47, 48], the regulation of O-GlcNAcylation on ciliogenesis could be

another mechanism by which altered O-GlcNAcylation can affect ADPKD. Elucidating the mechanisms by which O-GlcNAc is upregulated in ADPKD and alters cellular metabolism and ciliogenesis could reveal novel mechanisms and therapeutic targets.

In summary, our data demonstrate for the first time the role of IFT-A in an ADPKD context, revealing differential effects between nephron segments and between developing and mature renal microenvironments. Our findings also reveal for the first time that O-GlcNAcylation is increased in ADPKD. We propose that as a regulator of ciliary homeostasis and of the balance between glycolysis and oxidative phosphorylation, increased O-GlcNAc may drive certain key pathological processes in ADPKD.

Acknowledgements

We thank members of the KUMC Department of Anatomy and Cell Biology and the Jared Grantham Kidney Institute for helpful discussions. We thank Jing Huang of the KUMC Histology Core, which is supported by the Intellectual and Developmental Disabilities Research Center NIH U54HD090216 and NIH P30GM122731. We also thank Pat St. John and Larysa Stroganova of the KUMC Electron Microscopy Research Laboratory, which is supported by NIH P20GM104936. This work was also supported by a K-INBRE Summer Student Award to JTC (K-INBRE P20GM103418), the PKD Biomaterials and Biomarkers Repository Core in the Kansas PKD Research and Translational Core Center (NIH P30DK106912 to JPC), R01DK108433 to MS, and R01DK103033 to PVT.

Disclosures

The authors declare no conflict of interest.

Contributions

WW, LMS, MAK, HHW, TSP, BAA, DTJ, RD, JTC, AC, MTP, MS, DPW, and PVT performed experiments. WW, LMS, MAK, HHW, TSP, BAA, DTJ, RD, JTC, AC, MTP, MS, CS, DPW, JPC and PVT analyzed and interpreted data. WW, LMS, BAA, and PVT designed research. WW, LMS, and PVT wrote the manuscript. All authors revised and approved the final manuscript.

References

1. Lanktree, MB, Haghighi, A, Guiard, E, Iliuta, IA, Song, X, Harris, PC, Paterson, AD, Pei, Y: Prevalence Estimates of Polycystic Kidney and Liver Disease by Population Sequencing. *J Am Soc Nephrol*, 29**:** 2593-2600, 2018.
2. Torres, VE, Chapman, AB, Devuyst, O, Gansevoort, RT, Grantham, JJ, Higashihara, E, Perrone, RD, Krasa, HB, Ouyang, J, Czerwiec, FS: Tolvaptan in patients with autosomal dominant polycystic kidney disease. *N Engl J Med*, 367**:** 2407-2418, 2012.
3. Blair, HA: Tolvaptan: A Review in Autosomal Dominant Polycystic Kidney Disease. *Drugs*, 2019.
4. Torres, VE, Harris, PC: Mechanisms of Disease: autosomal dominant and recessive polycystic kidney diseases. *Nat Clin Pract Nephrol*, 2**:** 40-55; quiz 55, 2006.
5. Freedman, BS, Lam, AQ, Sundsbak, JL, Iatrino, R, Su, X, Koon, SJ, Wu, M, Daheron, L, Harris, PC, Zhou, J, Bonventre, JV: Reduced ciliary polycystin-2 in induced pluripotent stem cells from polycystic kidney disease patients with PKD1 mutations. *J Am Soc Nephrol*, 24**:** 1571-1586, 2013.
6. Cai, Y, Fedeles, SV, Dong, K, Anyatonwu, G, Onoe, T, Mitobe, M, Gao, JD, Okuhara, D, Tian, X, Gallagher, AR, Tang, Z, Xie, X, Lalioti, MD, Lee, AH, Ehrlich, BE, Somlo, S: Altered trafficking and stability of polycystins underlie polycystic kidney disease. *J Clin Invest*, 124**:** 5129-5144, 2014.
7. Walker, RV, Keynton, JL, Grimes, DT, Sreekumar, V, Williams, DJ, Esapa, C, Wu, D, Knight, MM, Norris, DP: Ciliary exclusion of Polycystin-2 promotes kidney cystogenesis in an autosomal dominant polycystic kidney disease model. *Nature communications*, 10**:** 4072, 2019.
8. Fu, W, Wang, L, Kim, S, Li, J, Dynlacht, BD: Role for the IFT-A Complex in Selective Transport to the Primary Cilium. *Cell reports*, 17**:** 1505-1517, 2016.
9. Mukhopadhyay, S, Wen, X, Chih, B, Nelson, CD, Lane, WS, Scales, SJ, Jackson, PK: TULP3 bridges the IFT-A complex and membrane phosphoinositides to promote trafficking of G protein-coupled receptors into primary cilia. *Genes Dev*, 24**:** 2180-2193, 2010.
10. Liem, KF, Jr., Ashe, A, He, M, Satir, P, Moran, J, Beier, D, Wicking, C, Anderson, KV: The IFT-A complex regulates Shh signaling through cilia structure and membrane protein trafficking. *J Cell Biol*, 197**:** 789-800, 2012.
11. Yoder, BK, Tousson, A, Millican, L, Wu, JH, Bugg, CE, Jr., Schafer, JA, Balkovetz, DF: Polaris, a protein disrupted in orpk mutant mice, is required for assembly of renal cilium. *American journal of physiology Renal physiology*, 282**:** F541-552, 2002.
12. Jonassen, JA, SanAgustin, J, Baker, SP, Pazour, GJ: Disruption of IFT complex A causes cystic kidneys without mitotic spindle misorientation. *J Am Soc Nephrol*, 23**:** 641-651, 2012.
13. Lin, F, Hiesberger, T, Cordes, K, Sinclair, AM, Goldstein, LS, Somlo, S, Igarashi, P: Kidney-specific inactivation of the KIF3A subunit of kinesin-II inhibits renal ciliogenesis and produces polycystic kidney disease. *Proc Natl Acad Sci U S A*, 100**:** 5286-5291, 2003.
14. Davis, EE, Zhang, Q, Liu, Q, Diplas, BH, Davey, LM, Hartley, J, Stoetzel, C, Szymanska, K, Ramaswami, G, Logan, CV, Muzny, DM, Young, AC, Wheeler, DA, Cruz, P, Morgan, M, Lewis, LR, Cherukuri, P, Maskeri, B, Hansen, NF, Mullikin, JC, Blakesley, RW, Bouffard, GG, Program, NCS, Gyapay, G, Rieger, S, Tonshoff, B, Kern, I, Soliman, NA, Neuhaus, TJ, Swoboda, KJ, Kayserili, H, Gallagher, TE, Lewis, RA, Bergmann, C, Otto, EA, Saunier, S, Scambler, PJ, Beales, PL, Gleeson, JG, Maher, ER, Attie-Bitach, T, Dollfus, H, Johnson, CA,

Green, ED, Gibbs, RA, Hildebrandt, F, Pierce, EA, Katsanis, N: TTC21B contributes both causal and modifying alleles across the ciliopathy spectrum. *Nat Genet*, 43**:** 189-196, 2011.

15. Srivastava, S, Molinari, E, Raman, S, Sayer, JA: Many Genes-One Disease? Genetics of Nephronophthisis (NPHP) and NPHP-Associated Disorders. *Front Pediatr*, 5**:** 287, 2017.
16. Tran, PV, Haycraft, CJ, Besschetnova, TY, Turbe-Doan, A, Stottmann, RW, Herron, BJ, Chesebro, AL, Qiu, H, Scherz, PJ, Shah, JV, Yoder, BK, Beier, DR: THM1 negatively modulates mouse sonic hedgehog signal transduction and affects retrograde intraflagellar transport in cilia. *Nat Genet*, 40**:** 403-410, 2008.
17. Qin, J, Lin, Y, Norman, RX, Ko, HW, Eggenschwiler, JT: Intraflagellar transport protein 122 antagonizes Sonic Hedgehog signaling and controls ciliary localization of pathway components. *Proceedings of the National Academy of Sciences of the United States of America*, 108**:** 1456-1461, 2011.
18. Eggenschwiler, JT, Anderson, KV: Cilia and developmental signaling. *Annual review of cell and developmental biology*, 23**:** 345-373, 2007.
19. Ma, M, Tian, X, Igarashi, P, Pazour, GJ, Somlo, S: Loss of cilia suppresses cyst growth in genetic models of autosomal dominant polycystic kidney disease. *Nat Genet*, 45**:** 1004-1012, 2013.
20. Viau, A, Bienaime, F, Lukas, K, Todkar, AP, Knoll, M, Yakulov, TA, Hofherr, A, Kretz, O, Helmstadter, M, Reichardt, W, Braeg, S, Aschman, T, Merkle, A, Pfeifer, D, Dumit, VI, Gubler, MC, Nitschke, R, Huber, TB, Terzi, F, Dengjel, J, Grahammer, F, Kottgen, M, Busch, H, Boerries, M, Walz, G, Triantafyllopoulou, A, Kuehn, EW: Cilia-localized LKB1 regulates chemokine signaling, macrophage recruitment, and tissue homeostasis in the kidney. *EMBO J*, 37, 2018.
21. Legue, E, Liem, KF, Jr.: Tulp3 Is a Ciliary Trafficking Gene that Regulates Polycystic Kidney Disease. *Curr Biol*, 29**:** 803-812 e805, 2019.
22. Shao, L, El-Jouni, W, Kong, F, Ramesh, J, Kumar, RS, Shen, X, Ren, J, Devendra, S, Dorschel, A, Wu, M, Barrera, I, Tabari, A, Hu, K, Haque, N, Yambayev, I, Li, S, Kumar, A, Behera, TR, McDonough, G, Furuich, M, Xifaras, M, Lu, T, Alhayaza, RM, Miyabayashi, K, Fan, Q, Ajay, AK, Zhou, J: Genetic reduction of cilium-length by targeting intraflagellar transport 88 protein impedes kidney and liver cysts formation in mouse models of autosomal polycystic kidney disease. *Kidney Int*, 2020.
23. Wang, W, Allard, BA, Pottorf, TS, Wang, HH, Vivian, JL, Tran, PV: Genetic interaction of mammalian IFT-A paralogs regulates cilia disassembly, ciliary entry of membrane protein, Hedgehog signaling, and embryogenesis. *FASEB J*, 2020.
24. Tran, PV, Talbott, GC, Turbe-Doan, A, Jacobs, DT, Schonfeld, MP, Silva, LM, Chatterjee, A, Prysak, M, Allard, BA, Beier, DR: Downregulating hedgehog signaling reduces renal cystogenic potential of mouse models. *J Am Soc Nephrol*, 25**:** 2201-2212, 2014.
25. Jacobs, DT, Silva, LM, Allard, BA, Schonfeld, MP, Chatterjee, A, Talbott, GC, Beier, DR, Tran, PV: Dysfunction of intraflagellar transport-A causes hyperphagia-induced obesity and metabolic syndrome. *Dis Model Mech*, 9**:** 789-798, 2016.
26. Piontek, K, Menezes, LF, Garcia-Gonzalez, MA, Huso, DL, Germino, GG: A critical developmental switch defines the kinetics of kidney cyst formation after loss of Pkd1. *Nat Med*, 13**:** 1490-1495, 2007.
27. Brown, D, Lydon, J, McLaughlin, M, Stuart-Tilley, A, Tyszkowski, R, Alper, S: Antigen retrieval in cryostat tissue sections and cultured cells by treatment with sodium dodecyl sulfate (SDS). *Histochem Cell Biol*, 105**:** 261-267, 1996.
28. Takakura, A, Nelson, EA, Haque, N, Humphreys, BD, Zandi-Nejad, K, Frank, DA, Zhou, J: Pyrimethamine inhibits adult polycystic kidney disease by modulating STAT signaling pathways. *Hum Mol Genet*, 20**:** 4143-4154, 2011.

29. Yamaguchi, T, Pelling, JC, Ramaswamy, NT, Eppler, JW, Wallace, DP, Nagao, S, Rome, LA, Sullivan, LP, Grantham, JJ: cAMP stimulates the in vitro proliferation of renal cyst epithelial cells by activating the extracellular signal-regulated kinase pathway. *Kidney Int*, 57**:** 1460-1471, 2000.
30. Yamaguchi, T, Nagao, S, Wallace, DP, Belibi, FA, Cowley, BD, Pelling, JC, Grantham, JJ: Cyclic AMP activates B-Raf and ERK in cyst epithelial cells from autosomal-dominant polycystic kidneys. *Kidney Int*, 63**:** 1983-1994, 2003.
31. Talbot, JJ, Shillingford, JM, Vasanth, S, Doerr, N, Mukherjee, S, Kinter, MT, Watnick, T, Weimbs, T: Polycystin-1 regulates STAT activity by a dual mechanism. *Proc Natl Acad Sci U S A*, 108**:** 7985-7990, 2011.
32. Yamaguchi, T, Wallace, DP, Magenheimer, BS, Hempson, SJ, Grantham, JJ, Calvet, JP: Calcium restriction allows cAMP activation of the B-Raf/ERK pathway, switching cells to a cAMP-dependent growth-stimulated phenotype. *J Biol Chem*, 279**:** 40419-40430, 2004.
33. Rowe, I, Chiaravalli, M, Mannella, V, Ulisse, V, Quilici, G, Pema, M, Song, XW, Xu, H, Mari, S, Qian, F, Pei, Y, Musco, G, Boletta, A: Defective glucose metabolism in polycystic kidney disease identifies a new therapeutic strategy. *Nat Med*, 19**:** 488-493, 2013.
34. Weimbs, T, Talbot, JJ: STAT3 Signaling in Polycystic Kidney Disease. *Drug Discov Today Dis Mech*, 10**:** e113-e118, 2013.
35. Talbot, JJ, Song, X, Wang, X, Rinschen, MM, Doerr, N, LaRiviere, WB, Schermer, B, Pei, YP, Torres, VE, Weimbs, T: The cleaved cytoplasmic tail of polycystin-1 regulates Src-dependent STAT3 activation. *J Am Soc Nephrol*, 25**:** 1737-1748, 2014.
36. Torres, JA, Kruger, SL, Broderick, C, Amarlkhagva, T, Agrawal, S, Dodam, JR, Mrug, M, Lyons, LA, Weimbs, T: Ketosis Ameliorates Renal Cyst Growth in Polycystic Kidney Disease. *Cell metabolism*, 30**:** 1007-1023 e1005, 2019.
37. Leonhard, WN, Song, X, Kanhai, AA, Iliuta, IA, Bozovic, A, Steinberg, GR, Peters, DJM, Pei, Y: Salsalate, but not metformin or canagliflozin, slows kidney cyst growth in an adult-onset mouse model of polycystic kidney disease. *EBioMedicine*, 47**:** 436-445, 2019.
38. Flowers, EM, Sudderth, J, Zacharias, L, Mernaugh, G, Zent, R, DeBerardinis, RJ, Carroll, TJ: Lkb1 deficiency confers glutamine dependency in polycystic kidney disease. *Nature communications*, 9**:** 814, 2018.
39. Nie, H, Ju, H, Fan, J, Shi, X, Cheng, Y, Cang, X, Zheng, Z, Duan, X, Yi, W: O-GlcNAcylation of PGK1 coordinates glycolysis and TCA cycle to promote tumor growth. *Nature communications*, 11**:** 36, 2020.
40. Tian, JL, Qin, H: O-GlcNAcylation Regulates Primary Ciliary Length by Promoting Microtubule Disassembly. *iScience*, 12**:** 379-391, 2019.
41. Yu, F, Li, T, Sui, Y, Chen, Q, Yang, S, Yang, J, Hong, R, Li, D, Yan, X, Zhao, W, Zhu, X, Zhou, J: O-GlcNAc transferase regulates centriole behavior and intraflagellar transport to promote ciliogenesis. *Protein Cell*, 2020.
42. Gerakopoulos, V, Ngo, P, Tsiokas, L: Loss of polycystins suppresses deciliation via the activation of the centrosomal integrity pathway. *Life Sci Alliance*, 3, 2020.
43. Zheng, D, Wolfe, M, Cowley, BD, Jr., Wallace, DP, Yamaguchi, T, Grantham, JJ: Urinary excretion of monocyte chemoattractant protein-1 in autosomal dominant polycystic kidney disease. *J Am Soc Nephrol*, 14**:** 2588-2595, 2003.
44. Hwang, SH, Somatilaka, BN, Badgandi, H, Palicharla, VR, Walker, R, Shelton, JM, Qian, F, Mukhopadhyay, S: Tulp3 Regulates Renal Cystogenesis by Trafficking of Cystoproteins to Cilia. *Curr Biol*, 29**:** 790-802 e795, 2019.
45. Patel, V, Li, L, Cobo-Stark, P, Shao, X, Somlo, S, Lin, F, Igarashi, P: Acute kidney injury and aberrant planar cell polarity induce cyst formation in mice lacking renal cilia. *Hum Mol Genet*, 17**:** 1578-1590, 2008.

46. Moyer, JH, Lee-Tischler, MJ, Kwon, HY, Schrick, JJ, Avner, ED, Sweeney, WE, Godfrey, VL, Cacheiro, NL, Wilkinson, JE, Woychik, RP: Candidate gene associated with a mutation causing recessive polycystic kidney disease in mice. *Science*, 264**:** 1329-1333, 1994.
47. Hopp, K, Ward, CJ, Hommerding, CJ, Nasr, SH, Tuan, HF, Gainullin, VG, Rossetti, S, Torres, VE, Harris, PC: Functional polycystin-1 dosage governs autosomal dominant polycystic kidney disease severity. *J Clin Invest*, 122**:** 4257-4273, 2012.
48. Liu, X, Vien, T, Duan, J, Sheu, SH, DeCaen, PG, Clapham, DE: Polycystin-2 is an essential ion channel subunit in the primary cilium of the renal collecting duct epithelium. *eLife*, 7, 2018.
49. Besschetnova, TY, Kolpakova-Hart, E, Guan, Y, Zhou, J, Olsen, BR, Shah, JV: Identification of signaling pathways regulating primary cilium length and flow-mediated adaptation. *Curr Biol*, 20**:** 182-187, 2010.
50. Kim, JI, Kim, J, Jang, HS, Noh, MR, Lipschutz, JH, Park, KM: Reduction of oxidative stress during recovery accelerates normalization of primary cilia length that is altered after ischemic injury in murine kidneys. *Am J Physiol Renal Physiol*, 304**:** F1283-1294, 2013.
51. Upadhyay, VS, Muntean, BS, Kathem, SH, Hwang, JJ, Aboualaiwi, WA, Nauli, SM: Roles of dopamine receptor on chemosensory and mechanosensory primary cilia in renal epithelial cells. *Front Physiol*, 5**:** 72, 2014.
52. Nikonova, AS, Plotnikova, OV, Serzhanova, V, Efimov, A, Bogush, I, Cai, KQ, Hensley, HH, Egleston, BL, Klein-Szanto, A, Seeger-Nukpezah, T, Golemis, EA: Nedd9 restrains renal cystogenesis in Pkd1-/- mice. *Proc Natl Acad Sci U S A*, 111**:** 12859-12864, 2014.
53. Husson, H, Moreno, S, Smith, LA, Smith, MM, Russo, RJ, Pitstick, R, Sergeev, M, Ledbetter, SR, Bukanov, NO, Lane, M, Zhang, K, Billot, K, Carlson, G, Shah, J, Meijer, L, Beier, DR, Ibraghimov-Beskrovnaya, O: Reduction of ciliary length through pharmacologic or genetic inhibition of CDK5 attenuates polycystic kidney disease in a model of nephronophthisis. *Hum Mol Genet*, 2016.
54. Cruz, NM, Song, X, Czerniecki, SM, Gulieva, RE, Churchill, AJ, Kim, YK, Winston, K, Tran, LM, Diaz, MA, Fu, H, Finn, LS, Pei, Y, Himmelfarb, J, Freedman, BS: Organoid cystogenesis reveals a critical role of microenvironment in human polycystic kidney disease. *Nat Mater*, 16**:** 1112-1119, 2017.
55. Nigro, EA, Distefano, G, Chiaravalli, M, Matafora, V, Castelli, M, Pesenti Gritti, A, Bachi, A, Boletta, A: Polycystin-1 Regulates Actomyosin Contraction and the Cellular Response to Extracellular Stiffness. *Scientific reports*, 9**:** 16640, 2019.
56. Miceli, C, Roccio, F, Penalva-Mousset, L, Burtin, M, Leroy, C, Nemazanyy, I, Kuperwasser, N, Pontoglio, M, Friedlander, G, Morel, E, Terzi, F, Codogno, P, Dupont, N: The primary cilium and lipophagy translate mechanical forces to direct metabolic adaptation of kidney epithelial cells. *Nature cell biology*, 22**:** 1091-1102, 2020.
57. Kiseleva, AA, Korobeynikov, VA, Nikonova, AS, Zhang, P, Makhov, P, Deneka, AY, Einarson, MB, Serebriiskii, IG, Liu, H, Peterson, JR, Golemis, EA: Unexpected Activities in Regulating Ciliation Contribute to Off-target Effects of Targeted Drugs. *Clin Cancer Res*, 25**:** 4179-4193, 2019.
58. Degrell, P, Cseh, J, Mohas, M, Molnar, GA, Pajor, L, Chatham, JC, Fulop, N, Wittmann, I: Evidence of O-linked N-acetylglucosamine in diabetic nephropathy. *Life Sci*, 84**:** 389-393, 2009.
59. Gellai, R, Hodrea, J, Lenart, L, Hosszu, A, Koszegi, S, Balogh, D, Ver, A, Banki, NF, Fulop, N, Molnar, A, Wagner, L, Vannay, A, Szabo, AJ, Fekete, A: Role of O-linked N-acetylglucosamine modification in diabetic nephropathy. *American journal of physiology Renal physiology*, 311**:** F1172-F1181, 2016.
60. Silva-Aguiar, RP, Bezerra, NCF, Lucena, MC, Sirtoli, GM, Sudo, RT, Zapata-Sudo, G, Takiya, CM, Pinheiro, AAS, Dias, WB, Caruso-Neves, C: O-GlcNAcylation reduces proximal tubule

protein reabsorption and promotes proteinuria in spontaneously hypertensive rats. *J Biol Chem*, 293**:** 12749-12758, 2018.

61. Xu, TH, Sheng, Z, Li, Y, Qiu, X, Tian, B, Yao, L: OGT knockdown counteracts high phosphate-induced vascular calcification in chronic kidney disease through autophagy activation by downregulating YAP. *Life Sci*, 261**:** 118121, 2020.
62. Feng, D, Sheng-Dong, L, Tong, W, Zhen-Xian, D: O-GlcNAcylation of RAF1 increases its stabilization and induces the renal fibrosis. *Biochim Biophys Acta Mol Basis Dis*, 1866**:** 165556, 2020.
63. Hu, J, Chen, R, Jia, P, Fang, Y, Liu, T, Song, N, Xu, X, Ji, J, Ding, X: Augmented O-GlcNAc signaling via glucosamine attenuates oxidative stress and apoptosis following contrast-induced acute kidney injury in rats. *Free Radic Biol Med*, 103**:** 121-132, 2017.
64. Ong, Q, Han, W, Yang, X: O-GlcNAc as an Integrator of Signaling Pathways. *Front Endocrinol (Lausanne)*, 9**:** 599, 2018.
65. Yu, F, Guo, S, Li, T, Ran, J, Zhao, W, Li, D, Liu, M, Yan, X, Yang, X, Zhu, X, Zhou, J: Ciliary defects caused by dysregulation of O-GlcNAc modification are associated with diabetic complications. *Cell Res*, 29**:** 171-173, 2019.

Figure Legends

Figure 1. Juvenile *Pkd2;Thm1* double knock-out mice have reduced cortical collecting duct cystic index, but not improved kidney function relative to *Pkd2* conditional knock-out mice. (A) Haemotoxylin and eosin staining of P21 kidney sections. Scale bar - 500μm. (B) Percent kidney weight/body weight (KW/BW) ratios, (C) Blood urea nitrogen (BUN) levels, (D) Percent cystic index, (E) Percent cortical cystic index, and (F) Percent medullary cystic index. *Pkd2* cko percent cystic indices are set at 1. Bars represent mean ± SD. In (B) and (C), statistical significance was determined by one-way ANOVA followed by Tukey's test. *p<0.05; ***p<0.001; ****p<0.0001; $^{\#\#\#\#}$p<0.0001 compared to Ctrl. In (D), (E) and (F), statistical significance was determined by unpaired two-tailed t-test. **p<0.01; ****p<0.0001. Each data point represents a mouse. (G) Staining of kidney cortex with LTL, THP and DBA. Scale bar - 100μm (H) Percent LTL+ dilations (I) DBA+ percent cystic index in renal cortex. *Pkd2* cko percent cystic indices are set at 1. Bars represent mean ± SD. Statistical significance was determined by unpaired two-tailed t-test. *p<0.05. (J) Haemotoxylin and eosin staining. Scale bar - 50μm (K) Area of Bowman's space/area of Bowman's capsule. Bars represent mean ± SD. Statistical significance was determined by one-way ANOVA followed by Tukey's test. ****p<0.0001; $^{\#\#}$p<0.01 compared to Ctrl; $^{\#\#\#\#}$p<0.0001 compared to Ctrl

Figure 2. Early onset *Pkd2* conditional knock-out and *Pkd2;Thm1* double knock-out kidneys have increased cell proliferation, inflammation and tubular epithelial cilia lengths. (A) Immunostaining of kidney cortex for PCNA (red) together with LTL or DBA (green). Scale bar - 10μm. (B) Percent PCNA+ cells per LTL+ and (C) DBA+ tubule. Each dot represents a tubule or a cyst from n=3 mice/genotype. Bars represent mean ± SD. Statistical significance was determined by Kruskal-Wallis test. ****p<0.0001; $^{\#}$p<0.05 compared to Ctrl; $^{\#\#\#}$p<0.001 compared to Ctrl;

$^{####}$p<0.0001 compared to Ctrl; $^{\&}$P<0.05 compared to *Pkd2* cko Tubule; $^{\$}$P<0.05 compared to dko tubule. (D) Immunostaining of kidney cortex for αSMA and F4/80. Scale bar - 50μm. (E) Immunostaining of kidney cortex for acetylated α-tubulin (red) together with LTL (green). Scale bar - 10μm. (F) Quantification of cilia length of LTL+ cells. (G) Immunostaining of kidney cortex for acetylated α-tubulin and IFT81 together with DBA. Scale bar - 10μm. n=3 mice/genotype. Quantification of cilia length of cortical DBA+ cells. Bars represent mean ± SD. Statistical significance was determined by one-way ANOVA followed by Tukey's test. ****p<0.0001; $^{\#}$p<0.05 compared to Ctrl; $^{\#\#\#}$p< 0.001 compared to Ctrl; $^{\#\#\#\#}$p<0.0001 compared to Ctrl.

Figure 3. Early onset *Pkd2* conditional knock-out and *Pkd2;Thm1* double knock-out kidneys have increased ERK and STAT3 activation. (A) Immunofluoresence for P-ERK together with LTL or DBA. Scale bar - 50μm. (B) Quantification of P-ERK+ tubules and (C) P+ ERK intensity. Each dot represents a tubule or a cyst from n=3 mice/genotype. Statistical significance was determined by one-way ANOVA followed by Tukey's test. *p<0.05; $^{\#}$p<0.05 compared to Ctrl; $^{\#\#\#\#}$p<0.0001 compared to Ctrl. (D) Immunohistochemistry for P-STAT3. Bottom and lower panels show cortex and medulla, respectively. n=3 mice/genotype. Scale bar - 25μm.

Figure 4. Early onset *Pkd2* conditional knock-out and *Pkd2;Thm1* double knock-out kidneys have increased O-GlcNAc signaling. (A) Immunohistochemistry for O-GlcNAc; (B) OGT and (C) OGA. Bottom and lower panels show cortex and medulla, respectively. Scale bar - 25μm. n=3 mice/genotype.

Figure 5. *Thm1* deletion in late-onset ADPKD mouse models attenuates renal cystogenesis and cilia lengthening. (A) Histology and lectin staining of *Pkd1* cko kidney sections. Scale bar - 100μm.

(B) Histology and lectin staining of *Pkd2* cko kidney sections. Scale bar - 50μm. (C) KW/BW ratios and (D) BUN levels for *Pkd1* cko mice and (E, F) for *Pkd2* cko mice. Bars represent mean ± SD. Each dot represents an animal. Statistical significance was determined by one-way ANOVA followed by Tukey's test. *p<0.05; **p<0.01; ***p<0.001. (G) Immunostaining of *Pkd1* cko renal cortex for acetylated α-tubulin together with DBA. Scale bar - 10μm. Scanning electron micrographs of primary cilia. Scale bar – 1.5μm. n=3 mice/genotype. (H) Immunostaining of *Pkd2* cko renal cortex for acetylated α-tubulin together with DBA. Scale bar - 10μm. n=3/genotype. (I) Immunostaining for ARL13B of normal human kidney (NHK) and ADPKD renal sections. Scale bar - 10μm. n=3 for each NHK and ADPKD. (J) Quantification of renal cilia lengths of *Pkd1* cko mice, (K) *Pkd2* cko mice, and (L) NHK and ADPKD tissue. Cilia lengths were quantified from immunofluorescence experiments of (G, H, I). Significance was determined using one-way ANOVA followed by Tukey's test (J, K) or by an unpaired t-test (L). Bars represent mean ± SD. $^{###}$p< 0.001 compared to Ctrl; $^{####}$p<0.0001 compared to Ctrl; ****p<0.0001

Figure 6. *Thm1* deletion in late-onset *Pkd1* conditional knock-out mouse attenuates proliferation and inflammation. (A) Immunofluorescence for PCNA (red) together with DBA (green). Scale bar - 100μm. (B) Immunostaining for αSMA (red) and F4/80 (red). Scale bar - 50μm. (C) Immunostaining for P-ERK (red) together with LTL (green) or DBA (green). Scale bar - 50μm. (D) Immunohistochemistry for P-STAT3. n=3 mice/genotype. (E) qPCR for *Ccl2*. Statistical significance was determined by one-way ANOVA followed by Tukey's test. **p<0.01

Figure 7. *Thm1* deletion in late-onset *Pkd1* conditional knock-out mouse attenuates perturbation of O-GlcNAc signaling. (A) Immunohistochemistry for O-GlcNAc; (B) OGT and (C) OGA. Bottom and lower panels show cortex and medulla, respectively. Scale bar – 20μm. n=3 mice/genotype.

Figure 8. Model of role of IFT-A deficiency in ADPKD.

In an early-onset ADPKD mouse model, deletion of *Thm1* causes nephron segment-specific effects, attenuating cortical collecting duct (CD) cystogenesis, but worsening proximal tubular and glomerular dilations, without affecting kidney function, cilia length, inflammation, and ERK, STAT3, and O-GlcNAc signaling. In a late-onset ADPKD mouse model, deletion of *Thm1* improves kidney function and reduces cystogenesis, inflammation, cilia length, and ERK, STAT3, and O-GlcNAc signaling.

Supplemental Material

Figure S1. Kidney histology and function of late-onset *Thm1* conditional knock-out mice. (A) Renal histology and (B) BUN levels of 6 month-old mice from the *Pkd1;Thm1* colony and (C, D) from the *Pkd2;Thm1* colony. Scale bar - 250μm

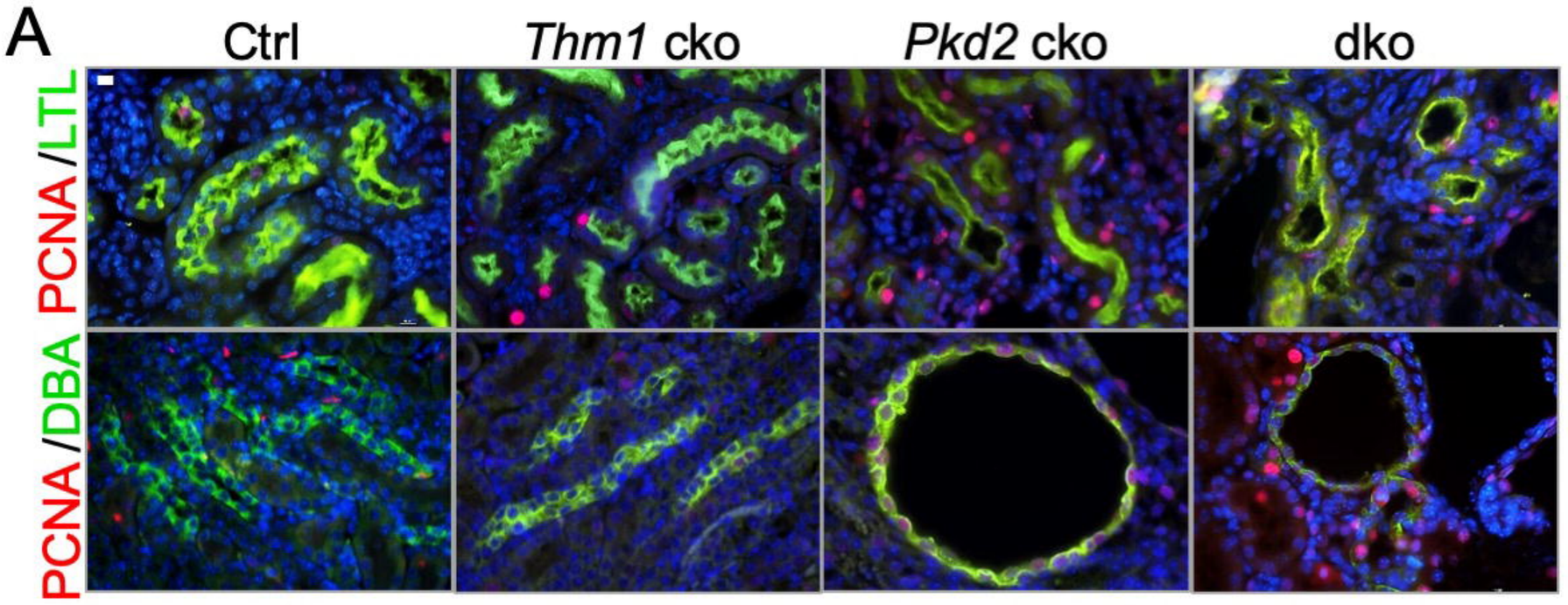

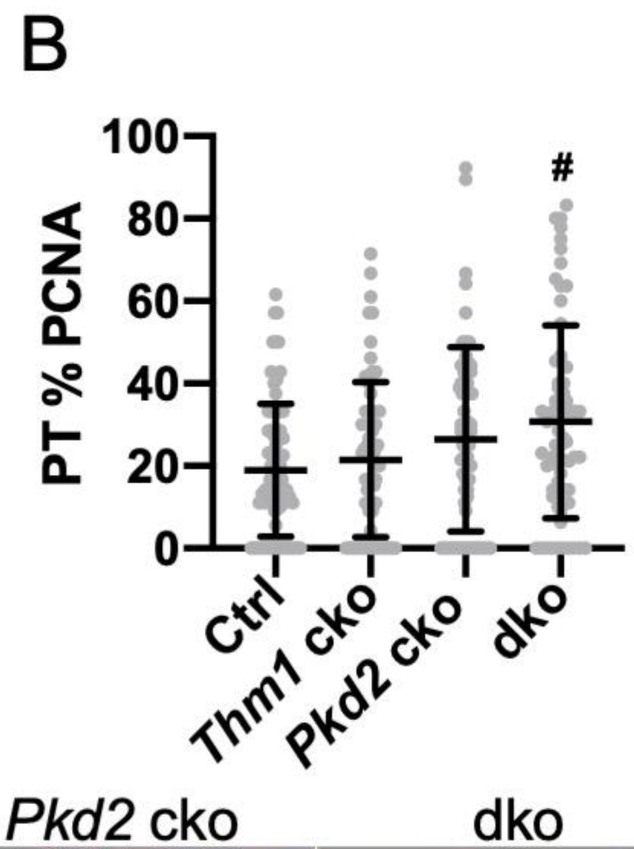

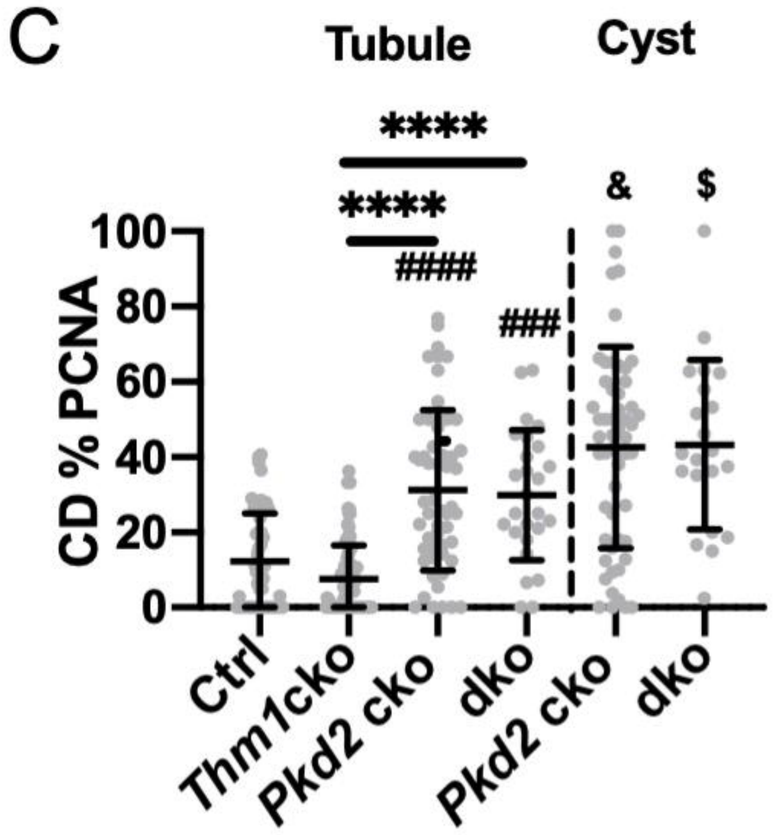

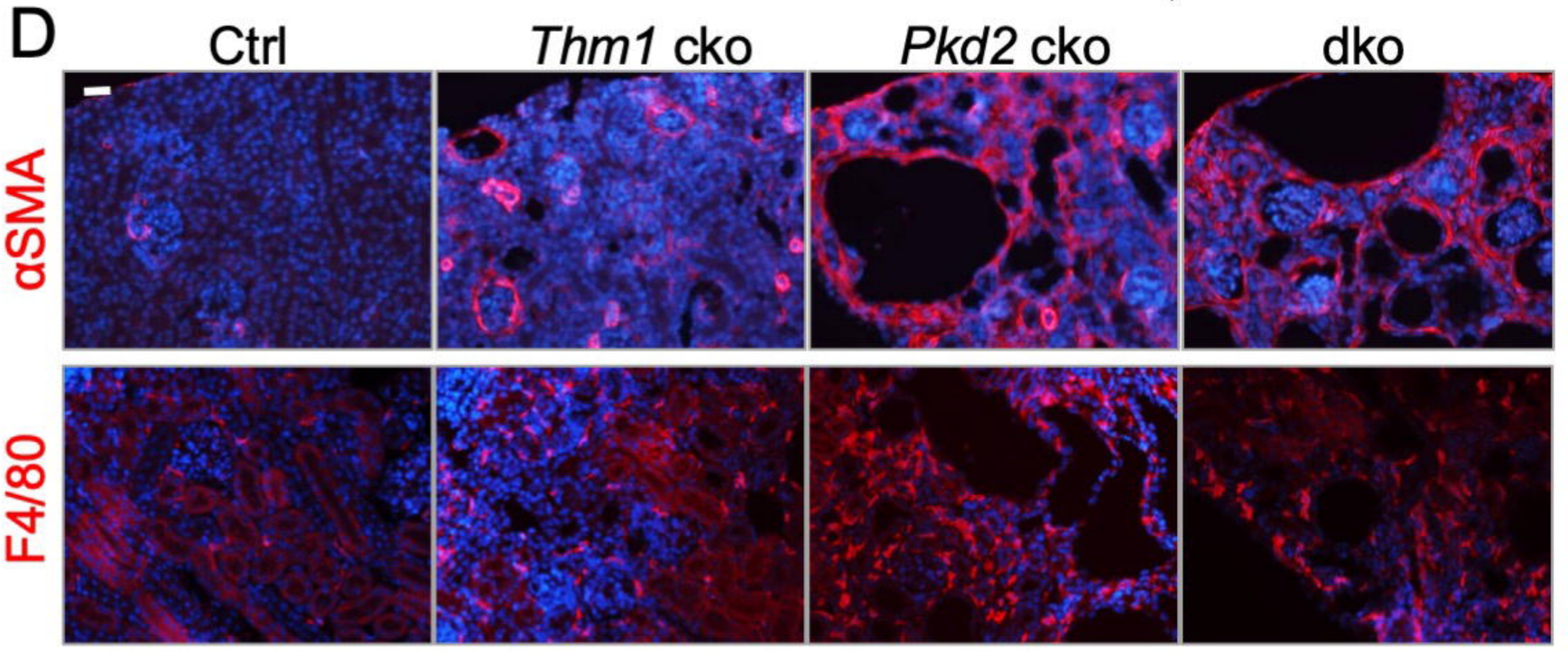

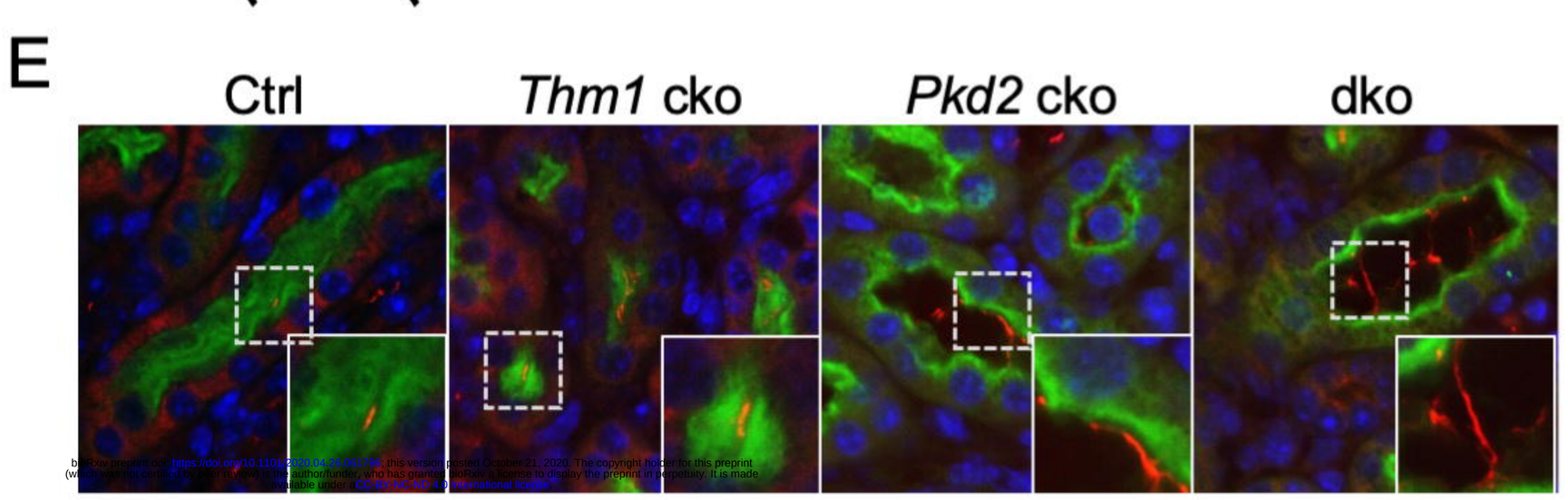

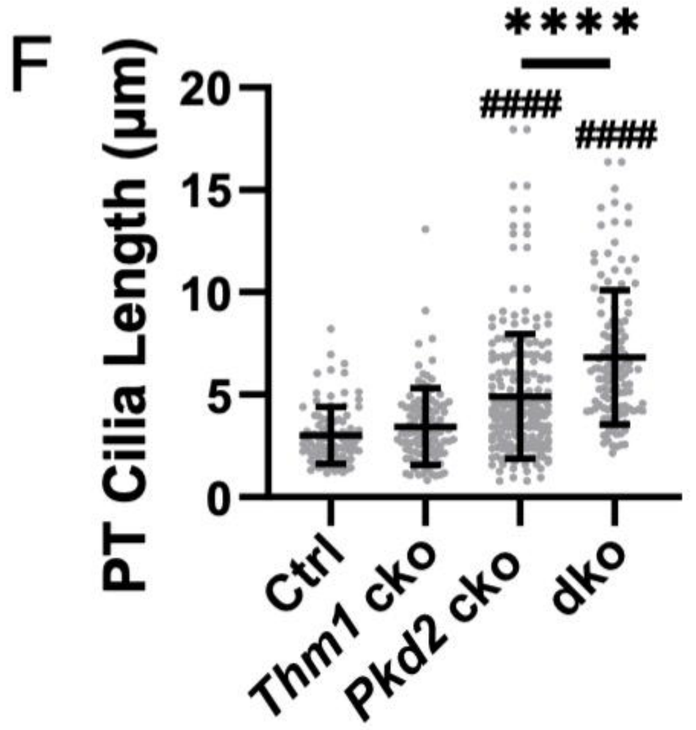

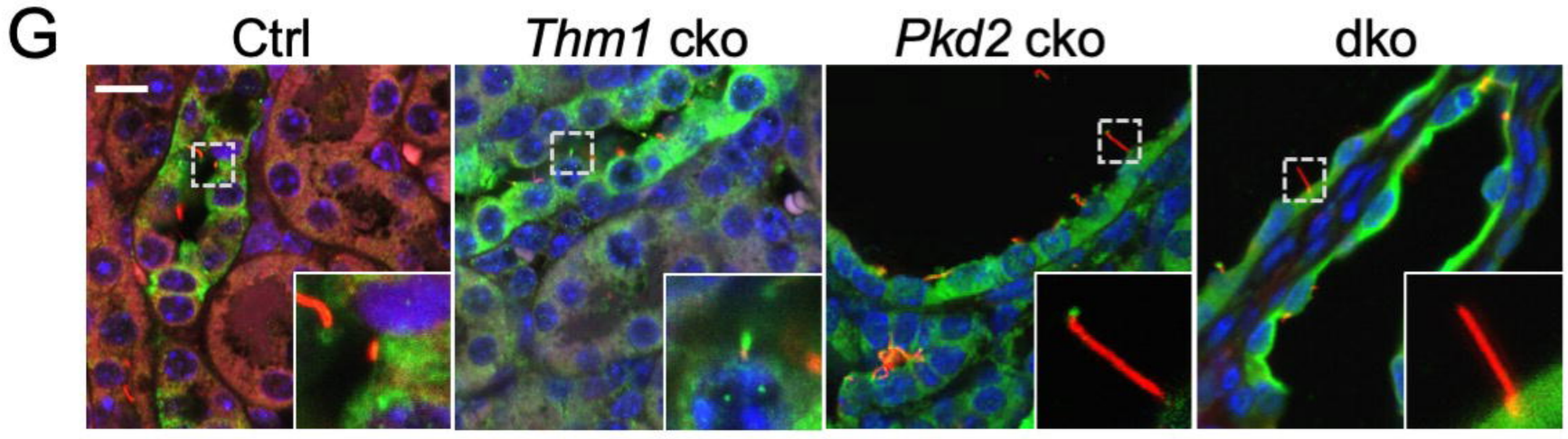

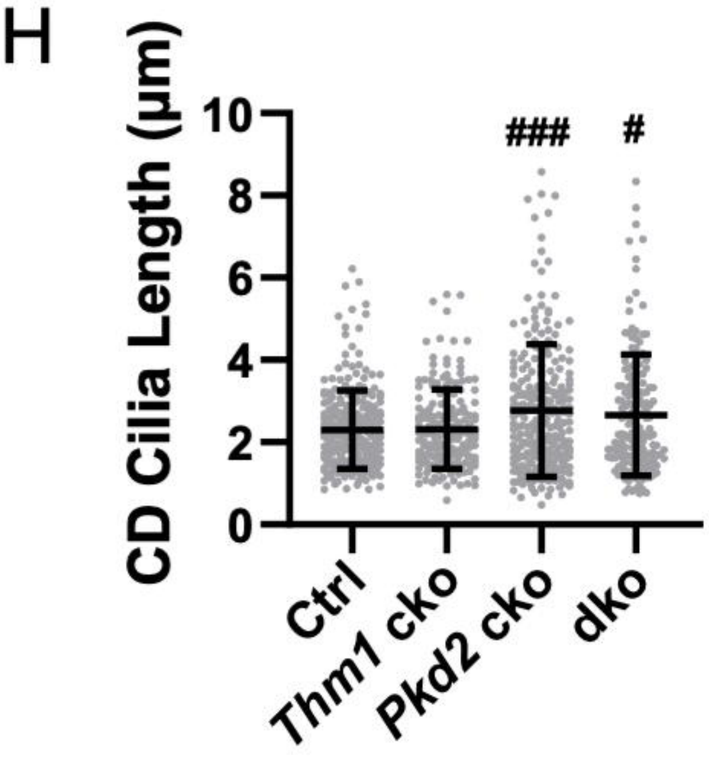

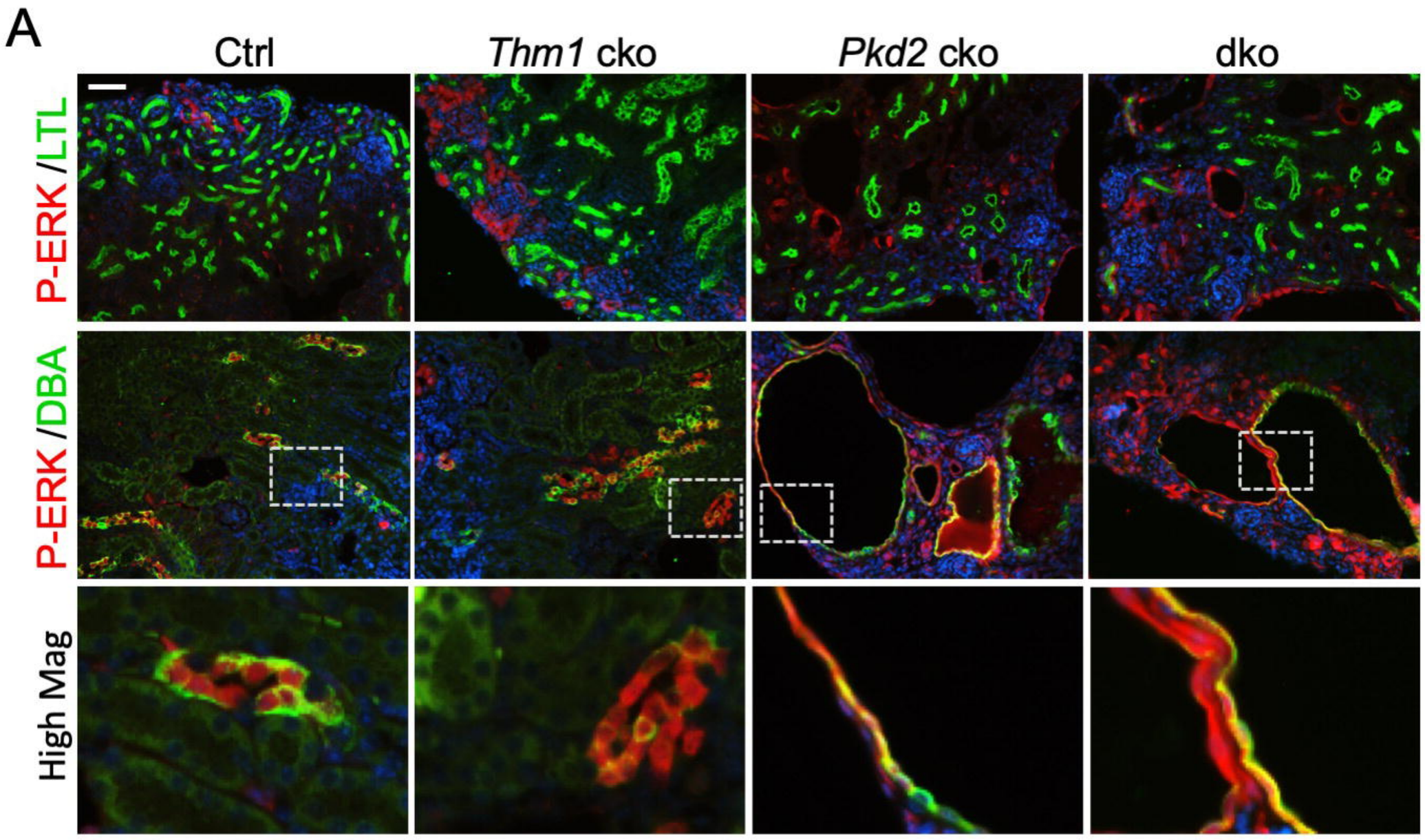

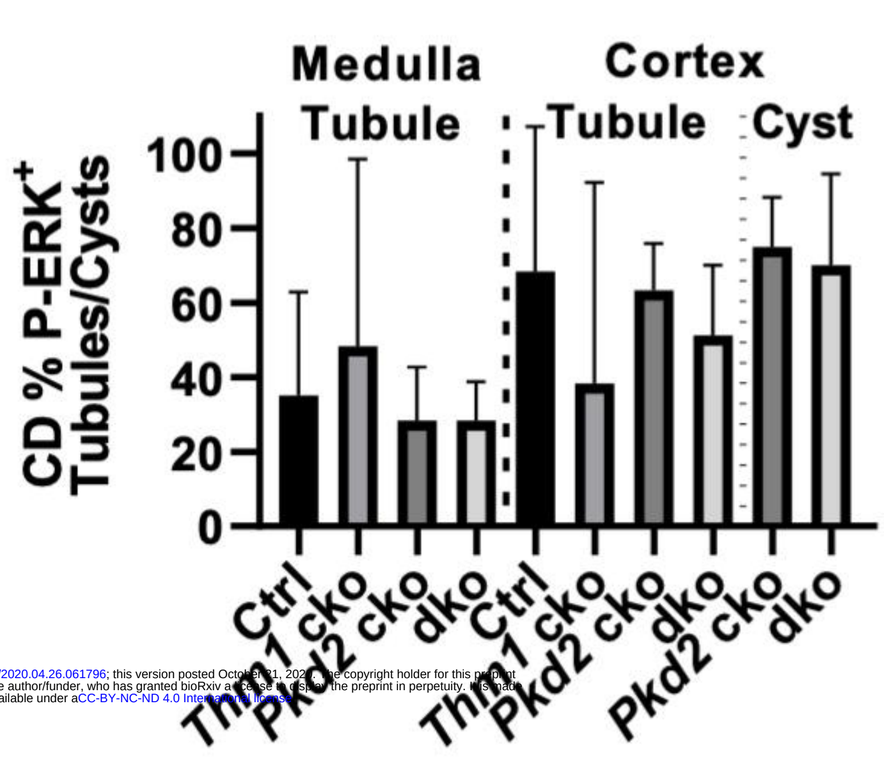

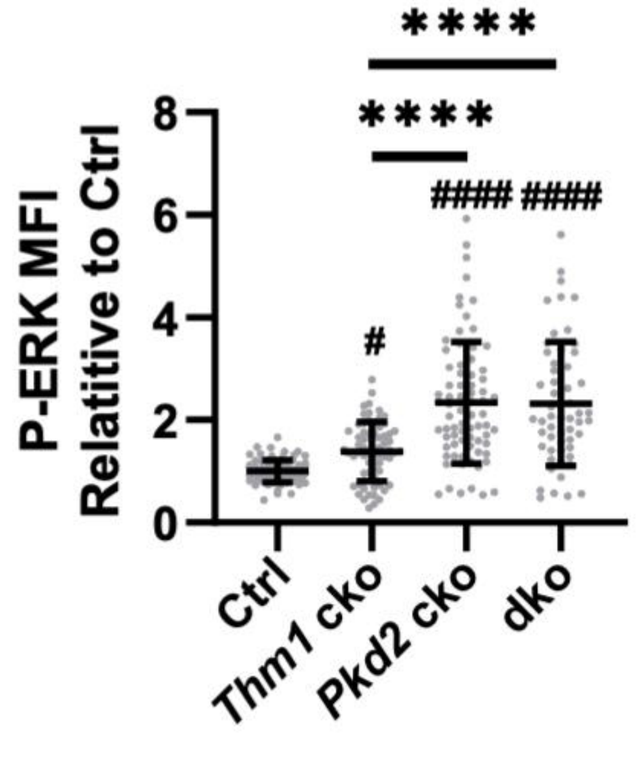

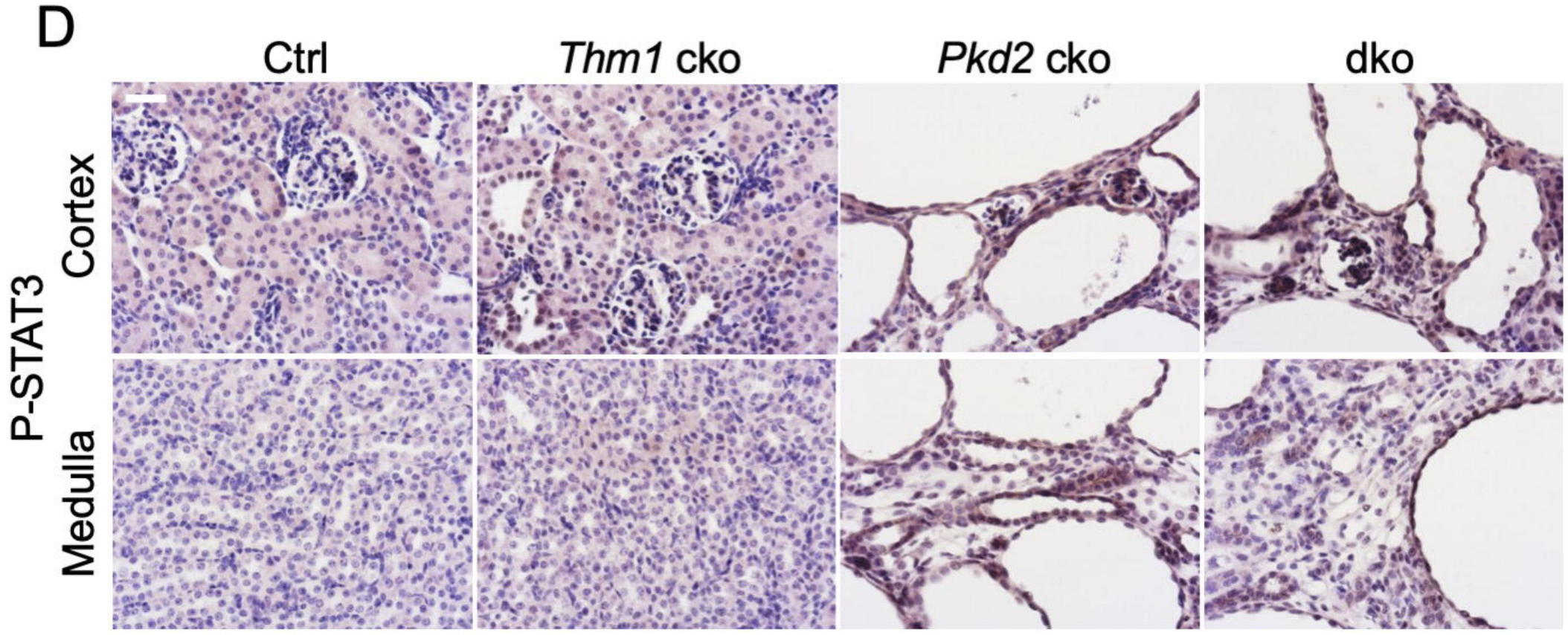

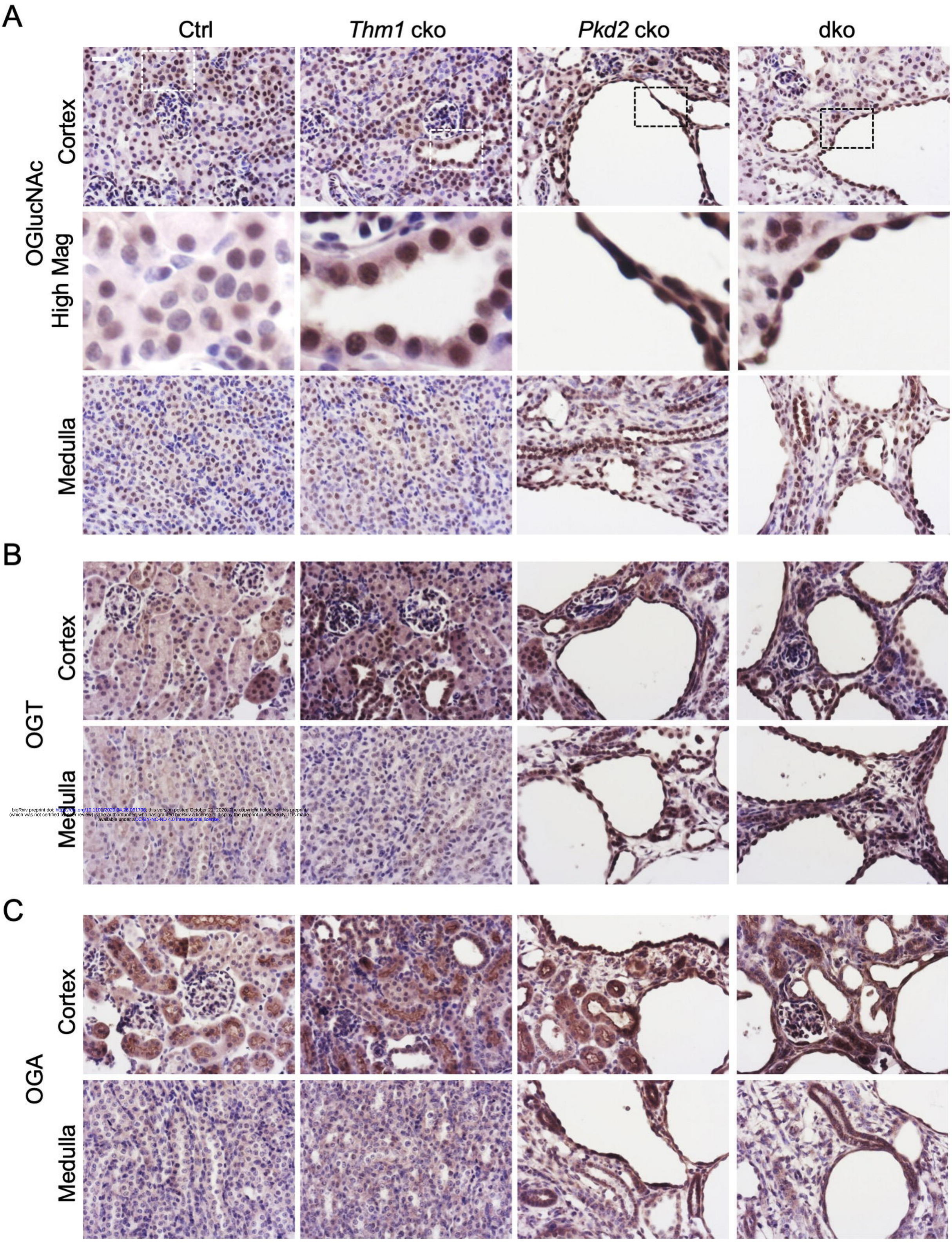

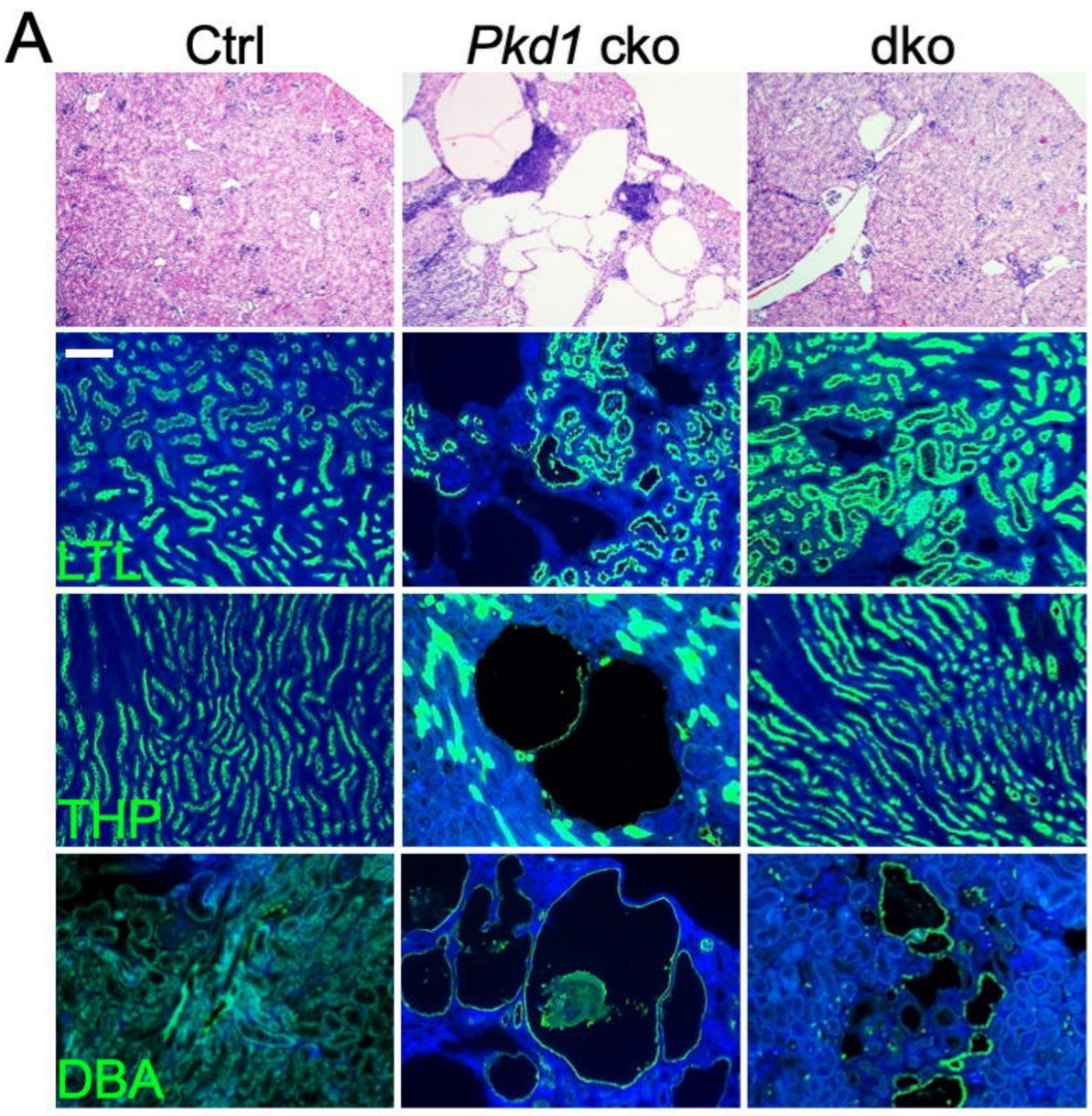

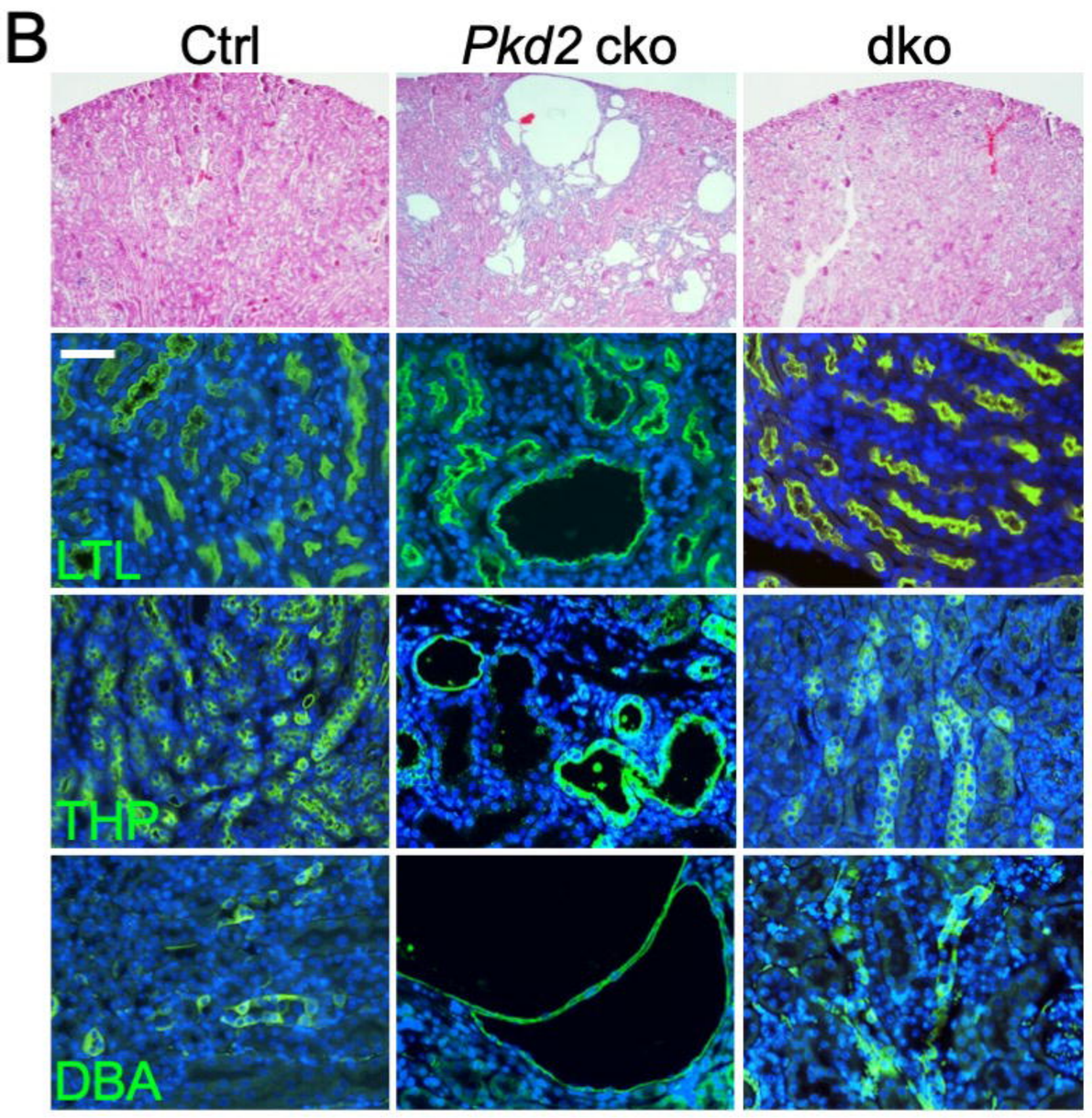

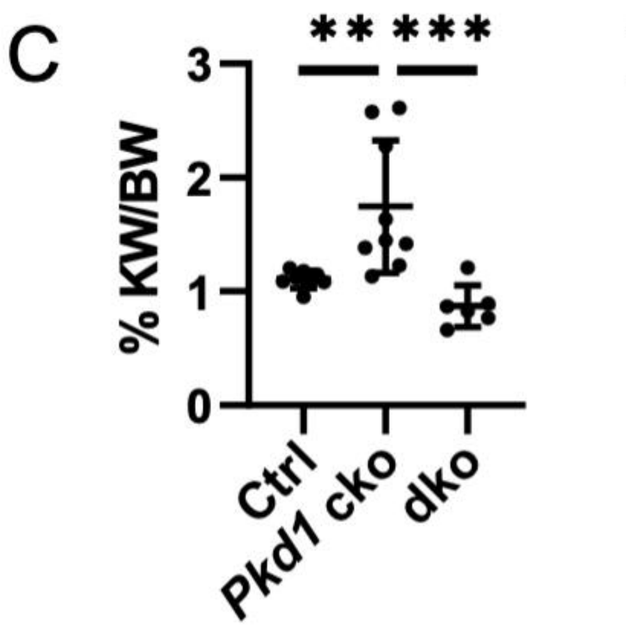

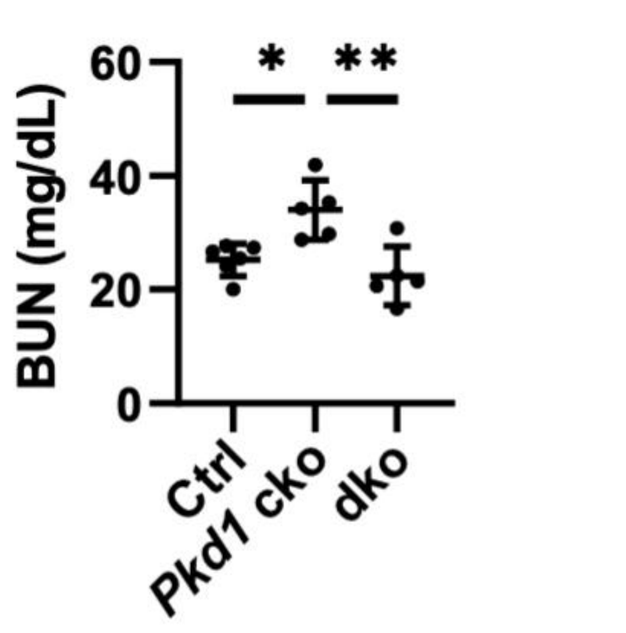

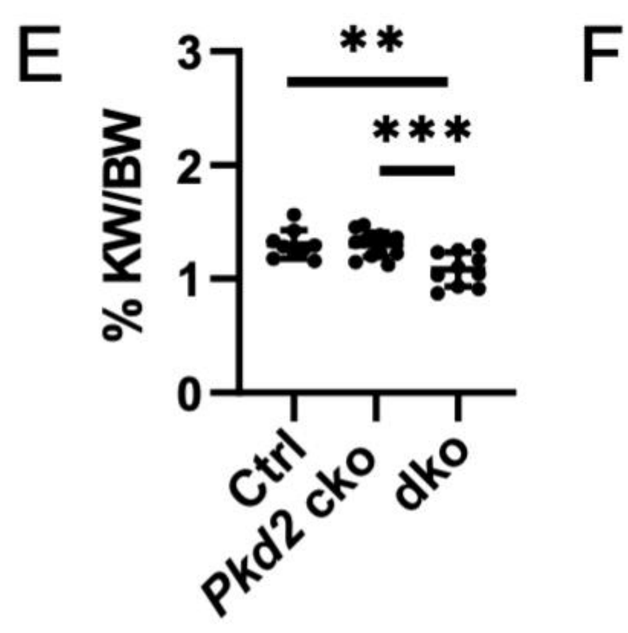

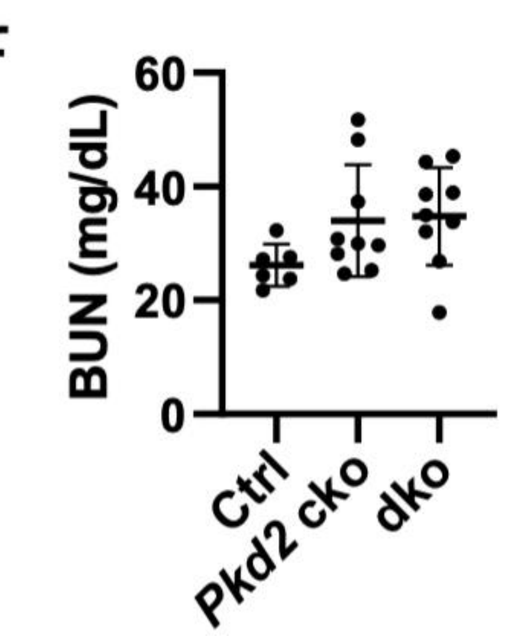

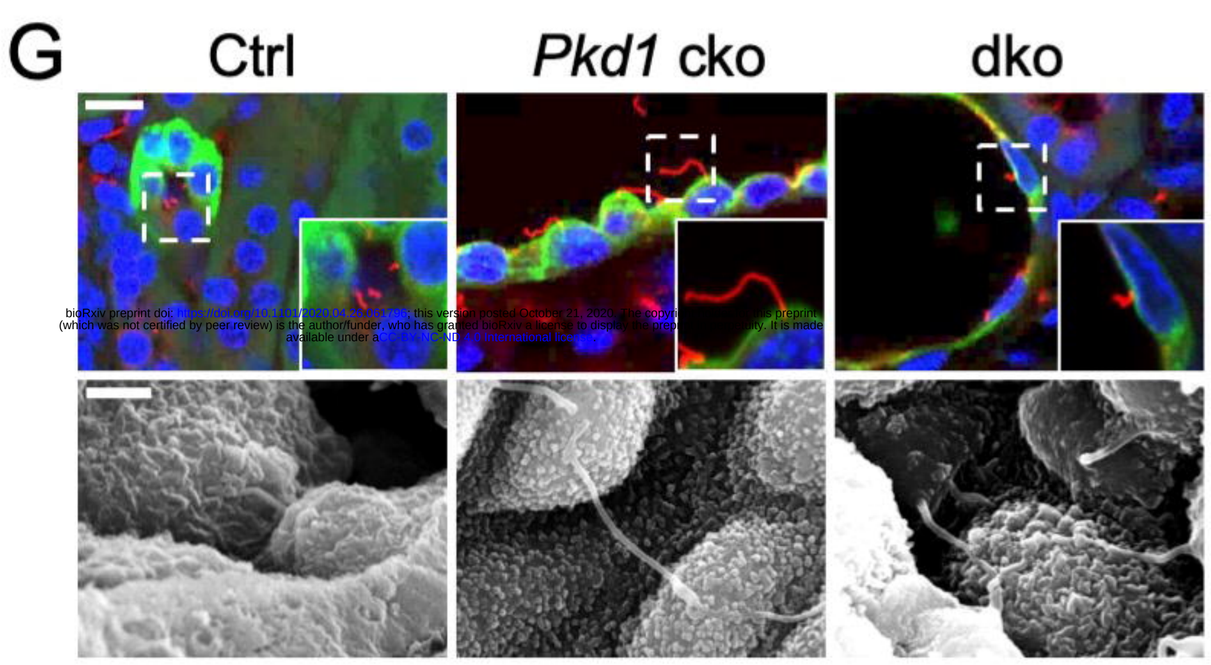

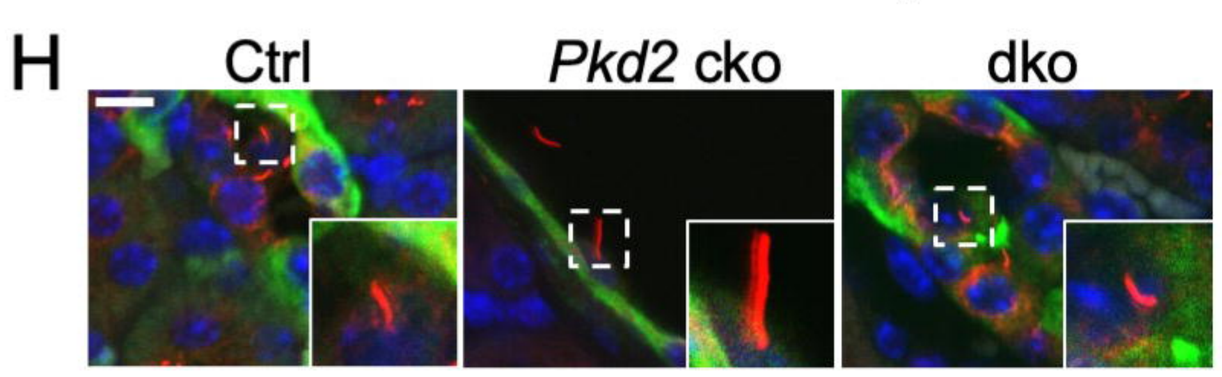

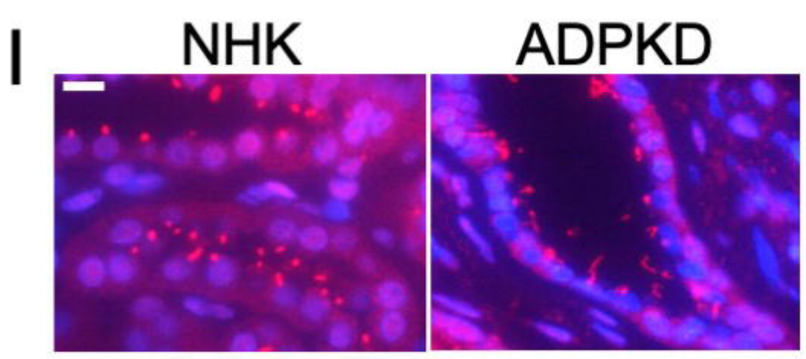

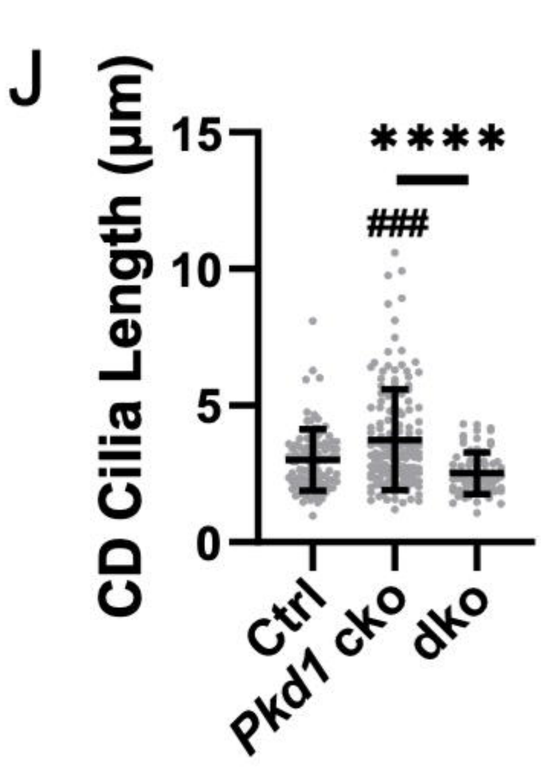

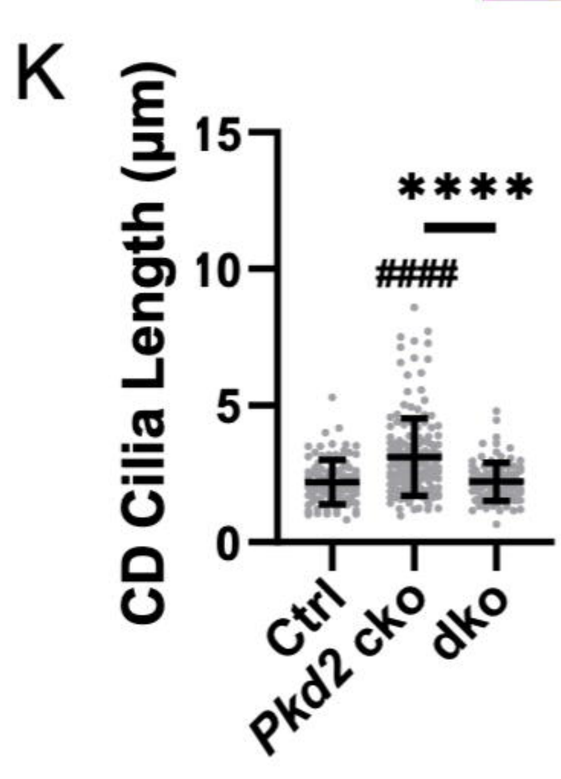

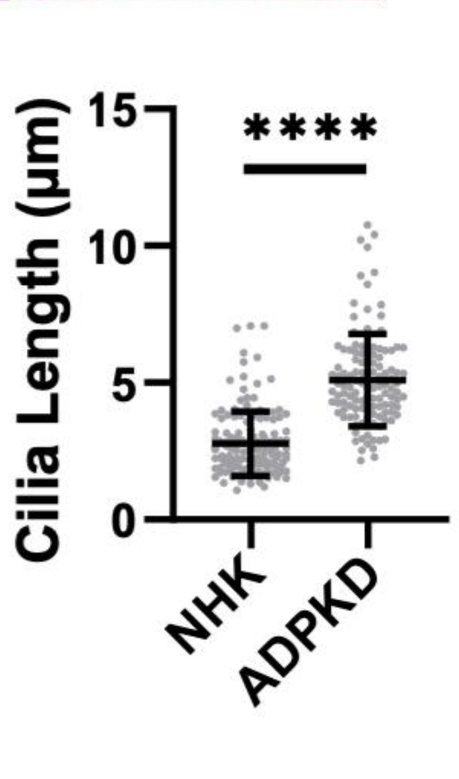

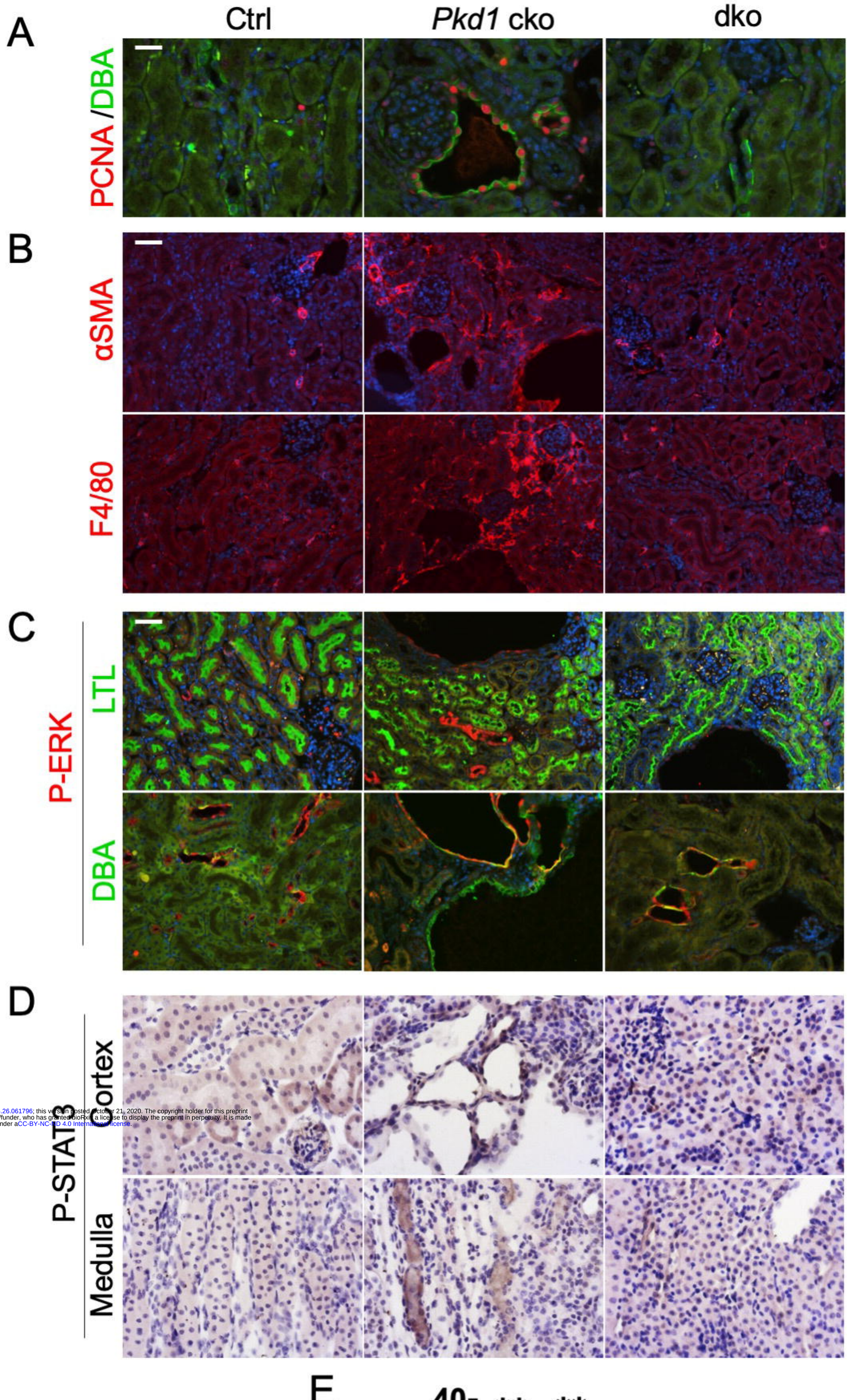

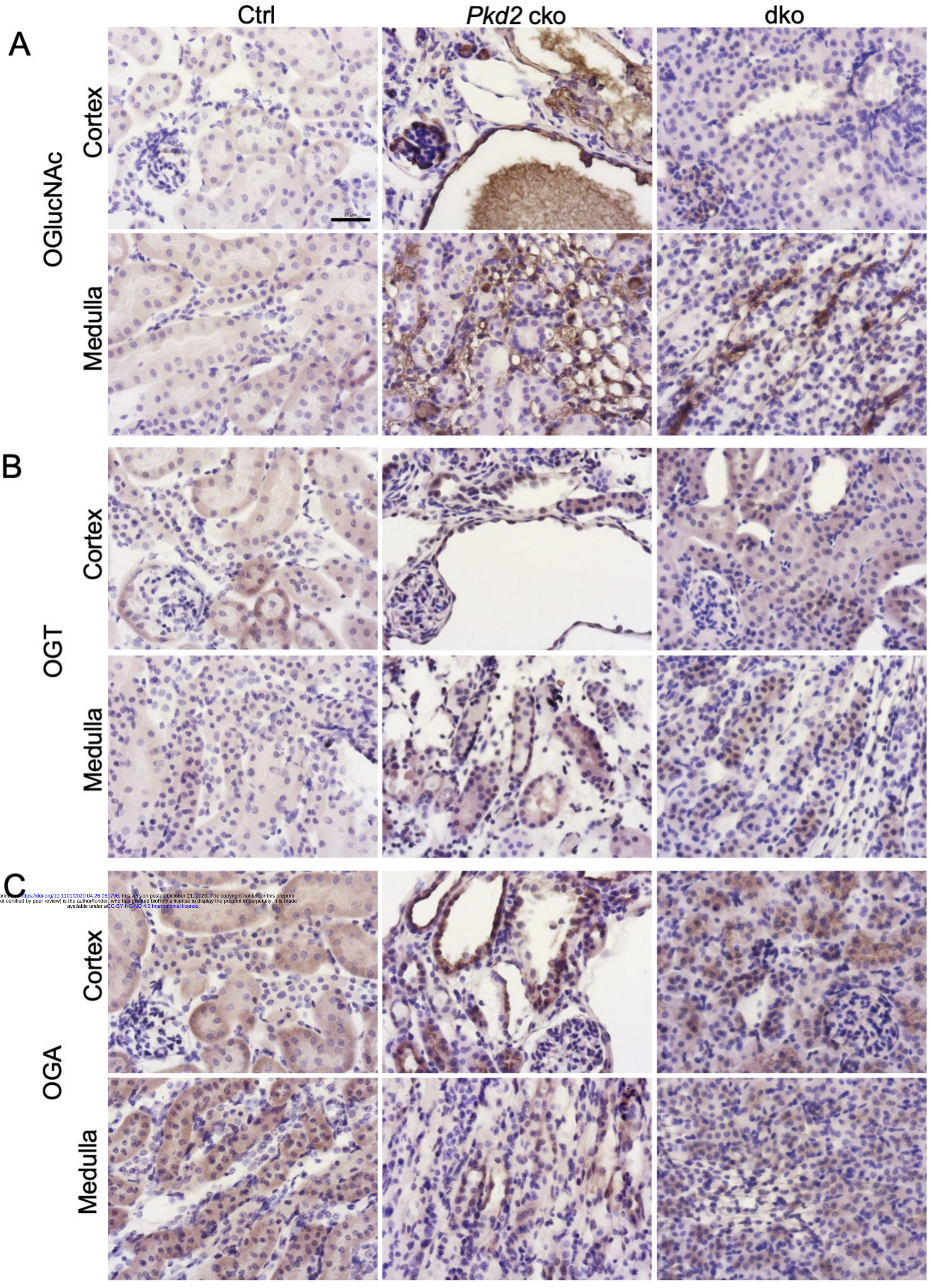

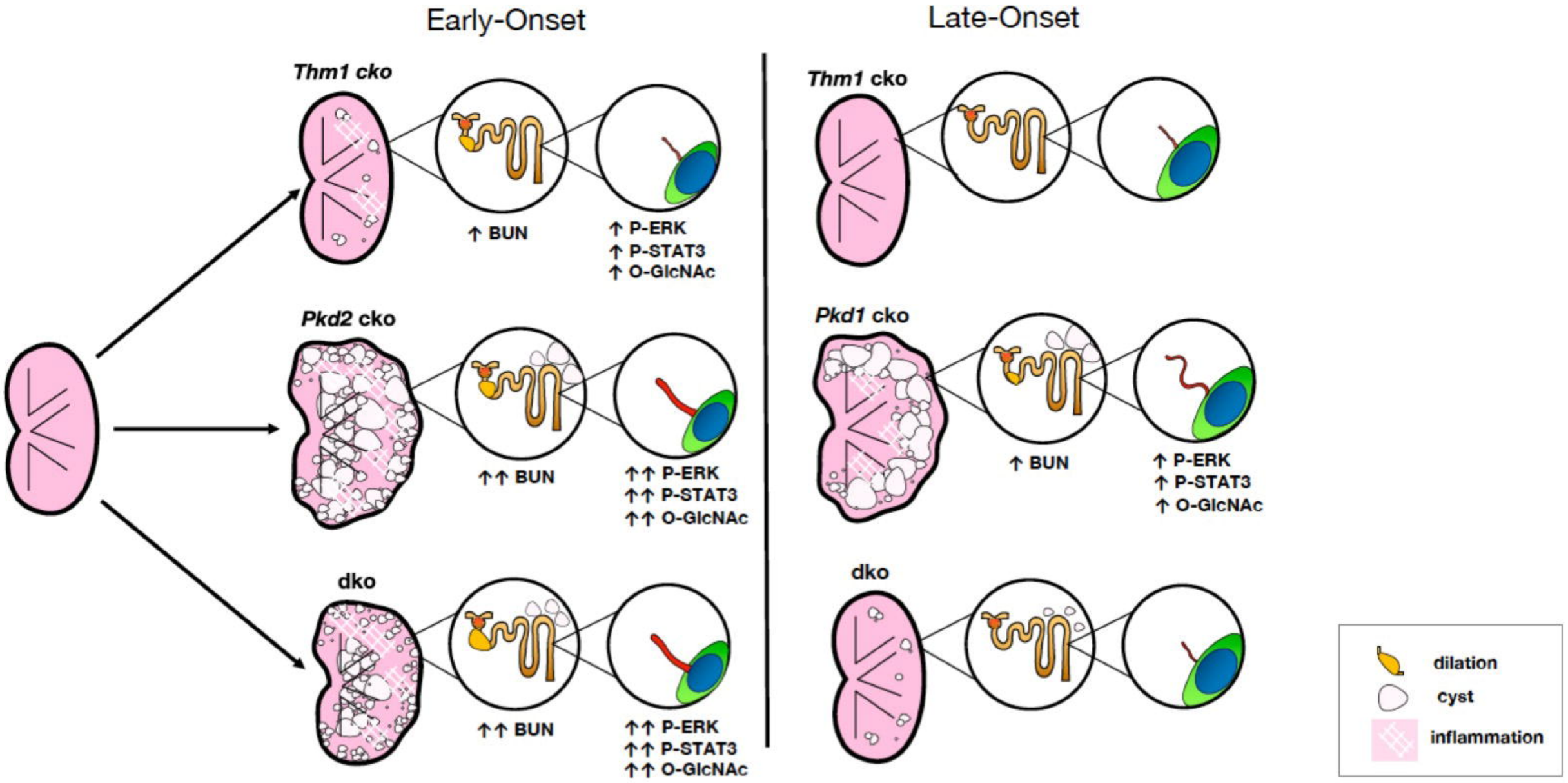

Fig S1